clean technologies

MDPI

Article

Optimizing the Hydrogen Supply Chain: Navigating Carbon Tax Scenarios for Fleet Decarbonization in Türkiye

Fidan Eser and Şule Itır Satoğlu *

Industrial Engineering Department, Faculty of Management, Istanbul Technical University, Maçka Şişli, İstanbul 34367, Türkiye; eser17@itu.edu.tr
* Correspondence: onbaslis@itu.edu.tr

Abstract

This study investigates how the hydrogen supply chain should be designed under alternative carbon tax scenarios to decarbonize heavy-duty freight transportation. A bi-objective, multi-period optimization model is developed to minimize the total daily system cost while constraining CO_2 emissions using the Augmented ε-constraint approach, thereby revealing the trade-off between economic and environmental objectives. The model was applied to Türkiye's heavy-duty transportation sector and solved under zero, moderate, and aggressive carbon tax scenarios. The results show that the levelized cost of hydrogen (LCOH) ranges from 2.06 to 14.06 \$/kg H_2. High carbon pricing increases the LCOH by 29.06% in hybrid designs, while raising the renewable energy share from 2.04% to 46.97% in centralized supply chains. Sensitivity analysis reveals that a ±20% variation in electrolyzer-based production costs does not alter the network topology but shifts the LCOH between 13.10 and 15.02 \$/kg H_2 in emission-focused solutions. The findings indicate that in renewable-energy-based decentralized structures, higher carbon tax policies primarily increase the LCOH. Still, the overall technology mix and network topology remain largely unchanged compared to the no-tax case. However, in centralized supply chains, carbon pricing affects both the energy sources and selected technologies. By integrating Türkiye's 2030–2053 policy milestones into a multi-period framework, this study distinguishes itself by providing a comprehensive, multi-period planning framework tailored to the economic and logistical realities of developing countries. Unlike existing models, our approach quantifies how evolving carbon tax trajectories decisively drive infrastructure investment by analyzing the direct impact of different tax levels on the operational and strategic decisions of heavy-duty transport. This research represents the first joint assessment of carbon tax policy instruments and the evolution of long-term hydrogen supply chains, offering a decision-making framework for policy-driven energy transitions in similar emerging economies.

Keywords: bi-objective optimization; hydrogen supply chain; supply chain; heavy-duty fuel-cell vehicle; carbon tax; carbon dioxide emission; fleet decarbonization; renewable energy

Check for updates

Academic Editor: Denitza Zgureva

Received: 7 April 2026
Revised: 19 May 2026
Accepted: 21 May 2026
Published: 2 June 2026

1. Introduction

The continuous growth in population and economic activity has led to a persistent increase in global energy demand. The widespread use of fossil fuels increases greenhouse gas emissions and accelerates climate change. Climate change has evolved into a global challenge affecting all countries, regardless of their level of development. International

 https://doi.org/10.3390/cleantechnol8030085

efforts to address this issue have been institutionalized through the United Nations Framework Convention on Climate Change (1992), the Kyoto Protocol, and the Paris Agreement. Under the Paris Agreement, limiting the increase in global average temperature to 2 °C and achieving a long-term carbon-neutral structure have been established as central objectives. Attaining these targets requires a fundamental transformation in patterns of energy production and consumption.

Given the global dominance of fossil fuel-based energy policies, the energy sector occupies a central position in this transformation. Greenhouse gas emissions from the energy sector account for nearly two-thirds of total global emissions [1]. In this context, electrification stands out as an important alternative to fossil fuel consumption.

In Türkiye, despite the strategic expansion of renewable capacity, electricity generation remains notably reliant on fossil fuels to ensure grid stability. According to the latest official statistics, as of 2025, 56.6% of Türkiye's electricity generation was derived from fossil sources (33.6% coal and 23% natural gas), while renewable energy sources accounted for 43.4% of total production [2]. This structure underscores that an electricity-centered transition alone remains insufficient to meet deep decarbonization targets.

Beyond the limited share of renewables, the inherent volatility of renewable energy sources poses a major technical challenge. Fluctuations in renewable output can significantly reduce electrolyzer operating efficiency and increase the LCOH. To address this, directly coupling renewable energy deployment with green hydrogen production is a practical solution. Utilizing surplus or curtailed electricity for water electrolysis not only provides a sustainable energy carrier but also helps manage the variability of natural resources. As Li et al. [3] noted, this integration is essential to overcome the intermittent nature of wind and solar power. While these macro-level perspectives are critical, the impact of resource volatility can also be managed through micro-level control strategies. For instance, Wang et al. [4] demonstrated that implementing flexible on-grid and off-grid mechanisms in electric–hydrogen-coupled microgrids can effectively mitigate energy fluctuations. This operational approach supports distributed production and offers a practical reference for energy integration efforts. Furthermore, implementing solutions such as thermal energy storage (TES) can mitigate these operational fluctuations. This improves electrolyzer efficiency and enhances the overall economics of renewable-based hydrogen production, especially in regions with a high share of fossil fuels, such as Türkiye [5].

The focus on heavy-duty vehicles (HDVs) is justified by their dominant role in both energy consumption and greenhouse gas emissions. Globally, energy use in transport accounts for approximately 16.2% of total emissions, making it one of the largest contributors alongside the industrial sector [6]. Within this framework, the transport sector is identified as the second-largest source of CO_2 emissions globally, with road transport being the most carbon-intensive mode [7]. According to the European Environment Agency, road transport alone was responsible for 73% of all EU transport GHG emissions in 2023 [8]. The impact of HDVs becomes even more pronounced when the freight sector is analyzed specifically. Data indicates that heavy-duty vehicles can account for up to 78.5% of freight-related carbon emissions, whereas light vans, maritime, and rail contribute significantly lower shares of 13.3%, 6.8%, and 1.1%, respectively [9]. Furthermore, hydrogen-fuel-cell technology is uniquely suited for the operational requirements of HDVs, providing the high energy density necessary for long-haul ranges and rapid refueling times that are currently unattainable with battery–electric alternatives for heavy freight logistics. These figures underscore that decarbonizing the heavy-duty segment through hydrogen transition is a prerequisite for achieving meaningful emission reductions in the transport sector.

In this framework, hydrogen is a promising energy carrier for reducing carbon emissions in the transportation sector. Hydrogen production capabilities from diverse primary energy sources, storability and transportability, zero carbon emissions at the point of use, and high energy density offer significant advantages, especially for heavy-duty freight applications. However, the long-term operational viability of these applications depends on overcoming technical challenges such as fuel cell performance degradation and durability issues. Factors such as electrode material degradation and catalyst loss, often exacerbated by fluctuating operating conditions, can shorten vehicle service life and increase maintenance and replacement costs [10]. Consequently, realizing this potential depends not only on the widespread adoption of fuel-cell vehicle technologies but also on comprehensive planning of the hydrogen supply chain infrastructure, including decisions on production locations, technologies, and capacities; transportation modes; and storage forms. Without coordinated infrastructure planning, the diffusion of hydrogen-fuel-cell vehicles will remain limited.

This transition process is particularly complex in developing countries. These countries, which often rely on natural gas and coal, may not be able to phase out fossil fuels immediately. So, it is necessary to address energy transformation not solely from an environmental perspective but also from the perspectives of economic sustainability and practical feasibility. This challenge is further validated by the recent report on the future of European competitiveness prepared by Mario Draghi [11]. The report demonstrates that even the European Union, one of the world's most advanced economic blocs, is experiencing a significant erosion of its competitive strength due to the costs of radical energy transitions, such as carbon taxes and hydrogen integration. In a context where even an innovation-leading region struggles to bear this weight, imposing similar policies on developing economies with limited financial depth and technological infrastructure may act as a "green barrier" that deepens global economic inequality. When the priorities of key stakeholders, such as governments, energy producers, and logistics companies, are disregarded, proposed plans become unrealistic. Approaches that focus exclusively on emission minimization may become infeasible due to high costs. In this regard, policy instruments such as carbon taxes, if designed in a balanced and context-sensitive manner, can encourage emission reductions while promoting cost-effective solutions. Nevertheless, as the European experience highlights, excessively high carbon tax levels may impose significant economic pressures on countries where industrialization is still ongoing.

For Türkiye, a developing country, the Energy and Natural Resources Ministry set clear targets in the Hydrogen Technologies Strategy and Roadmap for electrolyzer capacity for green hydrogen production and the levelized cost of hydrogen for 2030, 2035, and 2053 [12]. As these declared targets are significant, the optimal pathway planning for this hydrogen supply chain development requires in-depth analysis. To ensure policy alignment, the multi-period structure of this study (t1–t5) is designed to cover these national milestones, from the initial 2030 capacity targets to the 2053 net-zero vision.

In this context, Türkiye serves as a highly representative case for developing nations characterized by a dual-constraint energy landscape. As an emerging economy that has ratified the Paris Agreement, Türkiye has committed to ambitious emissions reduction targets; however, it remains dependent on a domestic energy structure heavily tied to fossil fuels, which cannot be phased out immediately without jeopardizing economic stability. This creates a fundamental challenge shared by many similar developing countries: how to design and implement transition policies that are both environmentally effective and practically feasible. Consequently, this research seeks to answer several strategic questions: How can a developing country plan a hydrogen transition that balances climate obligations with economic constraints? Specifically, how do different carbon tax trajectories influence infrastructure costs, technology selection, and emission reduction performance in the heavy-duty transport sector?

To address these questions, the primary objective of this study is to provide a long-term, integrated planning framework for hydrogen supply chain infrastructure to support the transition to hydrogen-fuel-cell vehicles in the heavy-duty freight transportation sector. For this purpose, a bi-objective, multi-period optimization model is proposed to minimize total daily system cost and carbon dioxide emissions simultaneously. The model integrates decisions on hydrogen production, transportation, and storage into a unified analytical framework and incorporates carbon taxes as a policy instrument that directly influences cost structures. This approach enables an examination of how the trade-off between cost and emissions evolves under different carbon tax levels and reveals the sensitivity of infrastructure decisions to policy conditions. The model is applied to the heavy-duty transportation sector in Türkiye to test its validity. The findings are promising for the feasible and policy-sensitive planning of hydrogen-based transportation infrastructure in developing countries.

The unique aspect of this study is that it proposes a hydrogen pathway planning framework for a heavy-duty fleet transition plan in the long run, considering alternative carbon tax policies, production, storage, and transportation methods, and energy sources, and reveals the trade-off between the costs and emission performance in different network architectures, and applies it to the case of Türkiye. The findings imply the impact of carbon tax policies on the feasibility of decarbonizing the transportation sector in this country.

The paper's organization is as follows: The second section reviews the literature. The third section explains the problem definition and methodology in detail. a case study for Türkiye is presented in the fourth section. The results of the case study are discussed, and the managerial implications are presented in the fifth section. Finally, the paper is concluded.

2. Literature Review

As decarbonization targets in road transportation become more clearly defined, hydrogen-fuel-cell vehicles gain strategic importance, particularly in the heavy-duty freight segment. In this segment, long driving ranges and high payload capacities are decisive factors. Battery-based solutions face substantial limitations due to weight, charging time, and infrastructure constraints. These conditions have led to the consideration of hydrogen not merely as an alternative fuel, but as an energy carrier considered at the system level. The literature supports this perspective by emphasizing that the role of hydrogen in transportation extends beyond vehicle technology, and that production, storage, transportation, and spatial configuration decisions jointly shape economic and environmental performance. Accordingly, research on hydrogen-based heavy-duty freight transport has progressively shifted from technology-specific production analyses toward integrated supply chain and network design approaches.

Studies adopting a more localized perspective on production have examined the technical feasibility of small-scale renewable energy-based systems. Dursun et al. [13] developed a dynamic model for Istanbul to simulate hydrogen production via electrolysis using a hybrid solar-and-wind energy system. Genç et al. [14] investigated the effects of electrolyzer capacity and wind turbine specifications on hydrogen production costs. This techno-economic perspective is further supported by studies on emerging markets such as Albania, which suggest that while renewable-based electrolysis currently faces high production costs (LCOH), a transition phase using natural gas with carbon capture could serve as a strategic bridge toward a long-term green hydrogen economy [15].

Research focusing on post-production stages addressed hydrogen storage from the perspectives of technical safety, site selection, and technology comparison. Rock salt formations in the Tuz Gölü region in Türkiye were assessed for large-scale hydrogen storage [16]. Another study evaluated alternative underground hydrogen storage options by incorporating technical, cost, socio-economic, and risk-related criteria [17]. Additionally, a study using a multi-criteria approach compared tank storage, metal hydride systems, and chemical storage alternatives [18]. Placing storage and safety at the center of the decision-making process, Kim and Moon [19] formulated a mixed-integer linear programming (MILP) model that incorporates production, storage, and multiple transportation modes, including pipelines. The results demonstrated that higher safety levels lead to more localized production structures and increased system costs. Kim et al. [20] proposed an index-based approach to evaluate the safety of hydrogen infrastructure by integrating production, storage, and transportation risks with regional characteristics. Their findings indicated that distributed production structures and liquid hydrogen transport generally exhibit lower overall risk.

Following these studies, integrated models that consider multiple elements of the hydrogen supply chain within a unified decision framework emerged. Almansoori and Shah [21] developed a single-period mixed-integer linear programming model that simultaneously considered decisions on hydrogen production, storage, and distribution. The study defined the hydrogen supply chain end-to-end and compared the effects of physical form choices on storage and transportation costs. In a subsequent study, Almansoori and Shah [22] extended this approach to a multi-period framework that incorporates long-term planning considerations. The study analyzed the development of the hydrogen infrastructure gradually over time in line with increasing demand, which was defined deterministically.

Multi-period supply chain models that jointly address temporal and spatial dimensions represent a significant maturation stage in hydrogen infrastructure planning. In this context, Agnolucci et al. [23] developed a multi-period Spatial Hydrogen Infrastructure Planning Model for the United Kingdom, integrating production, storage, transportation, and carbon capture and storage (CCS) infrastructure within the transportation sector. The study shows that demand density and geographic distribution play a key role in total system costs, and that a careful balance is essential between the lower production costs of large-scale centralized plants and rising transportation costs. Similarly, Moreno Benito et al. [24] examined the long-term development of hydrogen systems incorporating pipeline infrastructure and CCS technologies for the United Kingdom. The study showed that steam methane reforming (SMR) combined with CCS offers a cost-effective transition pathway and that pipeline investments become increasingly decisive as demand intensifies. Kim and Kim [25] analyzed the relationships among demand levels, network structures, and technology selection using a national-scale, multi-period model for South Korea that accounts for renewable energy sources. The results show that when hydrogen demand is low, centralized production structures based on biomass gasification are more economically attractive. However, as demand increases, more distributed network structures based on electrolysis facilities become economically favorable to reduce high transportation costs. This finding demonstrates that demand size directly affects capacity decisions, technology choice, and network configuration. While these spatial models analyze distributed structures at a macro level, integrating hydrogen into microgrid frameworks introduces an operational perspective on technology selection. For instance, Wang et al. [4] developed an electricity-hydrogen coupled microgrid control framework with a flexible on-grid and off-grid mechanism. Their study highlights how such distributed control systems can effectively manage fluctuations in renewable energy, offering a practical reference for stabilizing local hydrogen infrastructure during periods of supply volatility. In another national-scale and long-term study, Bique and Zondervan [26] developed a multi-period MILP model for Germany from 2030 to 2050, encompassing primary energy supply, hydrogen production, storage, and distribution. The results suggested that coal gasification plays a dominant role in the short term, while renewable energy-based electrolysis becomes more competitive in the long term as electricity prices decline. The distribution of liquid hydrogen via rail tankers was one of the most efficient options.

In studies that address cost and environmental objectives together, the impact of environmental constraints on technology selection and system design becomes more evident. The environmental potential of hydrogen extends beyond road transport as a cross-sectoral decarbonization pathway. In the maritime sector, life cycle assessments indicate that hydrogen internal combustion engines can reduce specific environmental burdens up to 99% compared to conventional diesel engines. However, the widespread adoption of these technologies still faces technical challenges regarding infrastructure gaps and low volumetric energy density [27]. Ogumerem et al. [28] examined the trade-offs between economic performance and greenhouse gas emissions using a multi-objective, multi-period model and solved it with the ε-constraint method. The study showed that selling oxygen, a by-product of electrolysis, can make this technology more competitive both economically and environmentally. Similarly, De Leon Almaraz et al. [29] proposed a multi-objective optimization framework that simultaneously incorporates cost, environmental impact, and safety risk, and defined alternative network structures corresponding to different priority combinations via Pareto frontiers. These studies represent an important methodological advancement by providing sets of solutions rather than a single optimal solution, allowing decision-makers to evaluate trade-offs among different objectives in hydrogen infrastructure planning.

Almansoori and Shah [30] addressed long-term uncertainty in hydrogen demand through a scenario-based, multi-stage, stochastic MILP framework. Their model integrated decisions on production, storage, distribution, and fueling-station location, comparing centralized production facilities with local production options. Nunes et al. [31] also adopted a two-stage stochastic programming approach to analyze liquid hydrogen supply chain configurations under demand uncertainty, showing that stochastic modeling yields more robust infrastructure designs than deterministic approaches. Dayhim et al. [32] incorporated demand uncertainty into a two-stage stochastic MILP model that simultaneously considered cost, emissions, energy consumption, and risk. Their results suggested that SMR offers cost advantages in early stages, while the gradual integration of electrolysis technologies reduces unit costs as demand increases.

A limited number of hydrogen supply chain design models explicitly integrated policy instruments. Almansoori and Betancourt-Torcat [33] analyzed the effects of the two primary policy instruments, namely a carbon tax and an emissions target, and of CCS technology on costs and emissions during hydrogen supply chain design. The emission factors from the production and distribution stages were treated as constraints. The study emphasizes that setting specific emission targets is a far more cost-effective strategy for policymakers than direct taxation. Similarly, Talebian et al. [34] directly integrated various policy instruments, such as production tax credits and capital incentives, into the design of the hydrogen supply chain to evaluate their effectiveness. The study found that the timing and gradual implementation of incentive policies play a more decisive role than the total subsidy amount. However, achieving these policy targets requires a reality check on the scale of investment. Analysis of energy transition scenarios in Colombia highlights a potential investment gap, in which a rapid energy transition may cost up to four to eight times more than official projections [35]. This underscores the necessity for more realistic and robust transition pathways. Although these studies demonstrate that policy instruments such as carbon taxes, emissions targets, and incentive mechanisms can directly influence hydrogen supply chain decisions, analyses of the long-term and cumulative effects of these instruments within a dynamic, multi-period framework remain limited in the literature.

In Türkiye, national-scale network design studies have provided important methodological contributions. Güler et al. [36] developed a model covering the period from 2021 to 2050, optimizing facility location and capacity expansion decisions to minimize total investment and operational costs. The results demonstrated that the network structure evolves from a centralized configuration toward a more distributed system as demand increases. However, the authors did not integrate the carbon emissions and renewable energy adoption as explicit objectives or constraints. Erdoğan et al. [37] proposed a single-period multi-objective MILP model for hydrogen-fuel-cell vehicle infrastructure in Türkiye, simultaneously minimizing cost, carbon emissions, and safety risks. Another long-term planning study proposed an optimization-based pathway for hydrogen infrastructure for the adoption of fuel-cell heavy-duty trucks in China, considering emission targets as constraints across alternative scenarios [38].

The literature review shows that although existing studies provide a methodological foundation for hydrogen infrastructure planning, there remains room for more comprehensive and dynamic frameworks to evaluate policy-sensitive, long-term transition strategies at the country level. This need is particularly evident in the heavy-duty transportation sector, where high demand intensity and long investment cycles require precise policy integration. In this context, Türkiye is selected as a representative case study for emerging economies characterized by a 'dual-constraint' energy landscape. As a signatory to the Paris Agreement with a 2053 net-zero target, Türkiye must navigate the challenge of decarbonizing its freight sector while managing a significant existing reliance on fossil fuels. By integrating hydrogen supply chain decisions with carbon-related policy instruments in this specific environment, our study seeks to provide a scalable model for how developing nations can balance climate obligations with economic and practical feasibility.

3. Methodology

This study designs the long-term configuration of a hydrogen supply chain to support the transition to hydrogen-fuel-cell vehicles in the heavy-duty road freight transportation sector. The proposed methodology is formulated as a multi-period, bi-objective mixed-integer linear programming (MILP) model. This framework jointly evaluates the infrastructure and operational decisions for hydrogen production, storage, and transportation under evolving demand and policy conditions. Two main objectives guide this decision problem. Minimizing the total cost of the hydrogen supply chain is the first objective. On the other hand, minimizing total carbon emissions from production, storage, and transportation is the second objective. Policy instruments such as carbon taxes influence the balance between these two objectives over time and reshape the feasible solution space. In this respect, the proposed multi-period, bi-objective decision model examines how the trade-off between cost and emissions objectives evolves and how supply chain structures change under different carbon tax scenarios.

The developed optimization model builds upon the widely used, multi-period hydrogen supply chain model of Almansoori and Shah [22]. This original model has a single-objective structure that minimizes the average total daily system cost. Our study extended the model defined in [22] to explicitly represent the environmental dimension by integrating a second objective function that minimizes carbon dioxide emissions, thereby transforming it into a bi-objective framework. In this way, the decision process is not limited to identifying the lowest-cost solution but also allows analysis of how the trade-off between cost and emissions objectives changes under different policy conditions. While the current model prioritizes a pure hydrogen supply chain tailored to heavy-duty road freight, the framework's structural design is intended to be robust and adaptable. It maintains the potential to incorporate more complex cross-sectoral coupling paradigms, such as the 'electro-hydrogen–ammonia' synergistic models proposed by Zhou et al. [39]. Integrating such multi-energy-flow synergies into the multi-period optimization could further enhance the model's practicality by evaluating ammonia as a high-density carrier or alternative fuel, thereby potentially mitigating trade-offs between economic and environmental objectives amid aggressive policy shifts. Figure 1 presents the general framework of the methodological steps followed in this study.

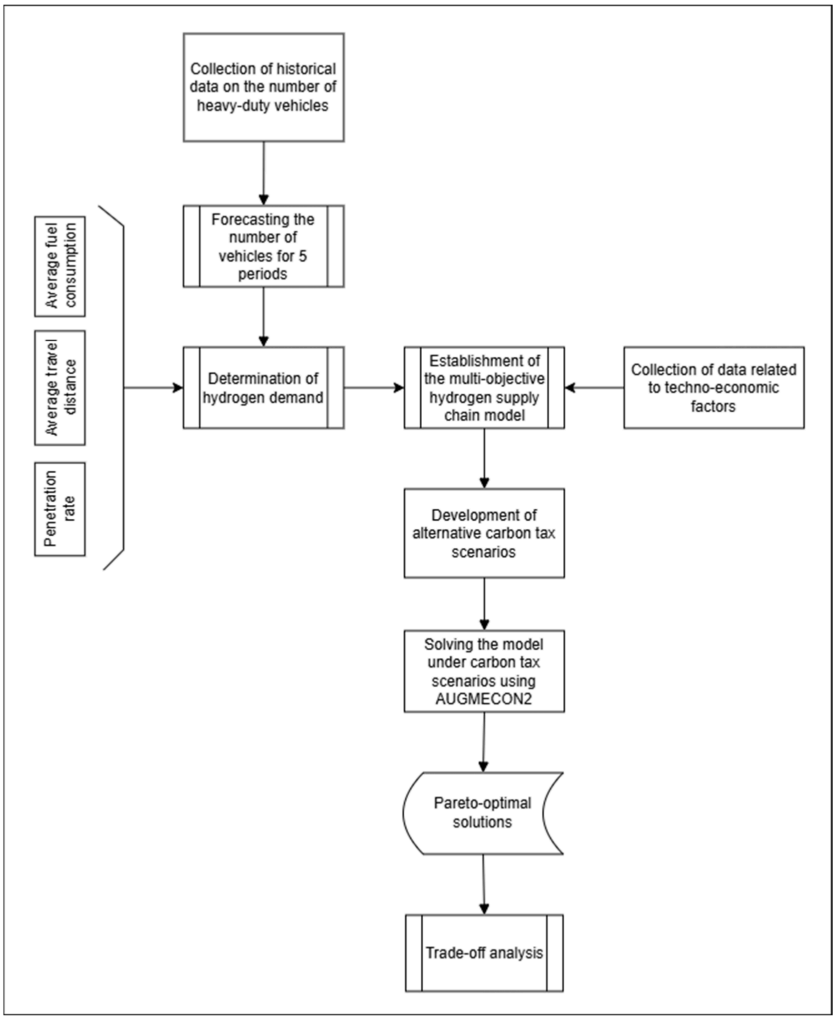

Figure 1. Methodological framework of the study.

The Methodology starts with the collection of historical data on the number of heavy-duty vehicles for the cities considered. Based on this data, the methodology forecasts the number of vehicles over the planning horizon. This step is called "demand forecasting". The planning horizon is divided into five strategic periods (t1 to t5), each representing a five-year interval. These periods are defined to align with the key phases of Türkiye's hydrogen transition [12]:

- t1 (2026–2030): Represents the initial integration phase, focusing on the national target of 2 GW electrolyzer capacity by 2030.
- t2–t4 (2031–2045): Covers the infrastructure expansion and industrial scale-up periods.
- t5 (2046–2050): Represents the final transition phase analyzed in this study, aligning with the strategic pathway toward the 2053 Net-Zero emission milestone.
- The following subsections explain the steps of the methodology.

3.1. Demand Forecasting

Hydrogen demand is estimated based on the number of heavy-duty vehicles operating in the freight transportation sector. First, data on the total number of heavy-duty vehicles in Türkiye and their average annual mileage are obtained from official statistics published by the Turkish Statistical Institute (TÜİK). Relying on these historical data, the Gray Forecasting method provides projections of the vehicle fleet through 2050, given their limited and uncertain nature. Using the projected number of vehicles, hydrogen demand for each cluster and period is calculated according to Equation (1). The estimation incorporates annual driving distance per vehicle, hydrogen consumption per kilometer, and the penetration rate of hydrogen-powered vehicles in the corresponding period, consistent with the assumptions adopted in previous studies [22,36,40].

$$D_{g,t} = ENV_{g,t} \times ATD \times AFC \times PR_t \tag{1}$$

In this equation, the annual hydrogen demand in cluster g during period t ($D_{g,t}$) is calculated based on the total number of vehicles expected to operate in the relevant cluster and period ($ENV_{g,t}$), the average annual driving distance per vehicle (ATD), and the hydrogen consumption per kilometer (AFC). The diffusion level of hydrogen-fuel-cell vehicles in the corresponding period is incorporated into the model through the period-specific penetration rate (PR_t). By jointly accounting for these components, hydrogen demand is treated as an exogenous input for each cluster and period and must be fully satisfied. The specific definitions, indices, and units for all parameters and variables associated with the demand estimation are explicitly detailed in Appendix A (Tables A1–A5).

3.2. Development of the Bi-Objective Hydrogen Supply Chain Model

The developed model conceptualizes the hydrogen supply chain as an integrated system that encompasses the entire process from production to final delivery at demand nodes and jointly optimizes production, storage, and transportation decisions. Owing to its multi-period, bi-objective MILP structure, the model determines in each period:

- facility establishment decisions;
- production quantities;
- storage infrastructure installations;
- inter-cluster transportation flows

simultaneously. Hydrogen demand is treated as exogenous for each cluster and period, and full demand satisfaction is enforced in every period. The physical flow of the hydrogen supply chain begins with primary energy sources and extends through production, transportation, and storage stages. Carbon dioxide emissions arising from these stages are internalized through a carbon tax mechanism and incorporated into the total system cost.

Formally, the bi-objective hydrogen supply chain model is developed based on the model of Almansoori and Shah [22] by incorporating an environmental objective and additional constraints, as explained below. To ensure a clear mathematical representation, the model's constraints are categorized into six functional groups: (1) demand constraints, (2) primary energy source constraints, (3) production plant constraints, (4) storage facility constraints, (5) transportation constraints, and (6) time evolution constraints. To provide full transparency without densifying the main text, the complete nomenclature—including sets, indices, parameters, and the explicit classification of decision variables as continuous, integer, or binary—is detailed in Appendix A (Tables A1–A5).

In the model, environmental performance is addressed at the system level, encompassing all major stages of the hydrogen supply chain. Total carbon emissions are defined as the aggregate of emissions arising from production, storage, and transportation activities. This approach enables a comprehensive assessment of the environmental implications of supply chain decisions across the entire system.

Production emissions in each period are calculated based on the amount of hydrogen produced in each cluster and period (P_{pjgt}), together with the emission coefficients associated with the primary energy sources used, as shown in Equation (2). Storage-related emissions in each period are determined by the number of storage facilities installed in the relevant period and region (NS_{sjgt}) together with the emission coefficients specific to each storage technology (Equation (3)). Transportation emissions in each period are computed using the number of transport units operating between clusters ($NTU_{lgg't}$), the distance between clusters ($AD_{gg'}$), and the emission coefficients corresponding to transportation processes (Equation (4)). The sum of these three components constitutes the objective function representing environmental performance in the model, namely, total carbon dioxide emission, as presented in Equation (5). When building the optimization model, the economic objective, the environmental objective, and the constraints expressed in [22] are all included. Hence, the model minimizes the total daily supply chain cost and total emissions. The specific definitions and indices for all parameters and variables mentioned above are provided in the comprehensive nomenclature in Appendix A (Tables A1–A5) to ensure the clarity and reproducibility of the mathematical structure. To build the entire model, the techno-economic data must be collected, as shown in Figure 1.

$$EM_t = \sum\nolimits_{p,j,g,e} P_{pjgt}\gamma_{epj}E_p \quad \forall t, \tag{2}$$

$$ES_t = \sum\nolimits_{s,j,g} NS_{sjgt}E_s \quad \forall t, \tag{3}$$

$$ET_t = \sum_{g,g',l,i} NTU_{lgg't}E_l AD_{gg'} \quad \forall t, \tag{4}$$

$$Minimize \sum_t (EM_t + ET_t + ES_t) \tag{5}$$

3.3. Development of Alternative Carbon Tax Scenarios

To examine the impact of carbon pricing on hydrogen supply chain decisions, this study defines three distinct carbon tax scenarios. The carbon tax levels are determined based on the study named Climate Mitigation Policy in Türkiye, developed by Parry et al. [41]. Tax levels are specified for each period in alignment with the model's five-period time structure. In Scenario 1, the carbon tax is zero for all periods. Scenario 2 introduces a moderate tax structure that increases gradually over time. Scenario 3 follows a more aggressive approach, characterized by a faster and higher escalation of carbon tax levels. The case study section presents the numerical values associated with the scenarios.

3.4. Scenarios Bi-Objective Model Solution Methodology

The model has two objective functions. The economic objective seeks to minimize the total daily system cost, while the environmental objective aims to minimize the total daily CO_2 emissions. The resulting bi-objective problem is solved using the AUGMECON2 method. This method is preferred over classical weighted-sum approaches to avoid the subjective scaling of economic and environmental objectives. Unlike simultaneous weighting, this approach ensures that all points on the Pareto-optimal front are identified with mathematical rigor, providing a more transparent and comprehensive trade-off analysis for policy makers. Within this framework, cost is treated as the primary objective function to be minimized, whereas emissions are incorporated into the model as a constraint through the ε parameter. By systematically varying the value of ε, the second objective value, Pareto-optimal solution sets are generated for each carbon tax scenario.

The AUGMECON2 method, developed by Mavrotas and Florios [42], is designed to generate the exact Pareto set for bi-objective decision-making problems. This approach incorporates structural enhancements designed to minimize the risk of producing weak Pareto solutions and to address the high computational costs often associated with the traditional constraint method. In implementing this method, the primary objective function (f_1) is minimized, while the remaining objectives (f_2,...,f_p) are incorporated into the model as specific constraints. Within this framework, the fundamental mathematical structure of AUGMECON2 is as follows:

$$min\left(f_1(x) + eps\left(\frac{S_2}{f_{2,max} - f_{2,min}} + 10^{-1}\frac{S_3}{f_{3,max} - f_{3,min}} + \ldots + 10^{-(p-2)}\frac{S_p}{f_{p,max} - f_{p,min}}\right)\right) \quad (6)$$

Subject to:

$$f_k(x) + S_k = f_{k,min} + i_k\left(\frac{f_{k,max} - f_{k,min}}{g_k}\right),\ k = 2, \ldots, p \quad (7)$$

$$x \in F, S_k \in R^+$$

Here, $f_k(x)$ represents the kth objective function of a p-objective model. In contrast, S_k denotes the surplus variables associated with the constrained objectives. The term eps is a sufficiently small coefficient, typically chosen between 10^{-6} and 10^{-3}, utilized to ensure lexicographical optimization. The values $f_{k,max}$ and $f_{k,min}$ correspond to the maximum and minimum values obtained from the payoff table for the respective objective functions. The range of change for a given objective ($r_k = f_{k,max} - f_{k,min}$) is divided into g_k equal intervals and $i_k(i_k = 0, 1, \ldots, g_k)$ serves as the interval counter for the current grid point. The details of the method are available in Mavrotas and Florios [42].

3.5. Trade-Off Analysis

After solving the model for the three scenarios using the AUGMECON2 Algorithm, several Pareto Optimal solutions are obtained. For an ultimate decision, a trade-off analysis is essential. During this analysis, one should assess the marginal improvement in the environmental objective at the expense of the economic objective. Additionally, the impact of the three carbon tax scenarios on supply chain development decisions over the planning horizon is analyzed extensively and compared to assess the effects of different carbon tax policies.

4. Case Study of the Proposed Model for Türkiye

This section presents a case study on the decarbonization of Turkish heavy-duty transportation based on fuel-cell vehicles for the years 2026–2050. For this purpose, the proposed bi-objective model is solved using parameters for heavy-duty vehicle number forecasts, expected hydrogen demand, all emission sources, cost components, and three levels of carbon taxes. The following subsections explain in detail the spatial aggregation of cities into clusters, data sources and assumptions, carbon tax scenarios, and penetration rates.

4.1. Spatial Aggregation and Distance Structure

The 81 provinces of Türkiye are grouped to achieve a more balanced spatial structure for the analysis of heavy-duty freight transportation. Provinces whose share of the national heavy-duty vehicle fleet is below 1% are merged with geographically adjacent provinces. As a result of this process, 28 clusters are defined and illustrated in Figure 2. Table A6 in the Appendix A presents the details of the clusters.

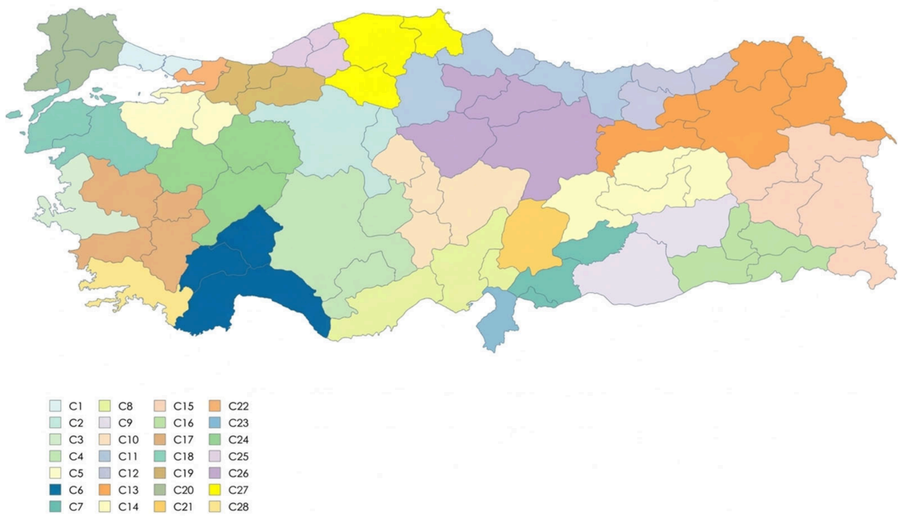

Figure 2. Cluster-Based Spatial Aggregation for Heavy-Duty Transport (28 clusters).

The cluster centers are calculated by averaging the latitudes and longitudes of the provinces included in each cluster. Distances between clusters are computed using the great-circle distances between their centers. To avoid assuming a zero distance for transportation within the same cluster, the diagonal elements of the distance matrix are set to intra-cluster distances. For clusters consisting of multiple provinces, the diagonal distance is set equal to the maximum great-circle distance between the provinces within that cluster. For clusters comprising a single province, the relevant province's approximate urban diameter is used. The distance matrix is presented in the Appendix A Table A7.

4.2. Data Sources and Assumptions

The dataset used in this study was constructed by combining Türkiye-specific energy, transportation, and geographical data with techno-economic parameters reported in the literature. Data on energy supply were compiled from the Energy Market Regulation Institution (EPDK) [43], the Energy Affairs General Directorate (BEPA) [44], and the Turkish Coal Enterprises (TKİ) [45], covering renewable energy resources, biofuels, natural gas, and coal potential. Data on heavy-duty vehicle stock and travel distances are obtained from the Turkish Statistical Institute (TÜİK) [46]. The techno-economic parameters used in the model, including investment and operating costs as well as technology-specific capacity parameters, are adopted from the study by Almansoori and Shah [22]. Emission factors and the emission accounting framework are based on the hydrogen supply chain emission model proposed by Ochoa Bique et al. [47]. Table 1 summarizes the main components of the dataset and their corresponding sources. Comprehensive technical parameters and specific numerical values for each category are further detailed in Tables A8–A14 in the Appendix A. To preserve the computational tractability of the model and to more clearly isolate the effects of policy scenarios, the following assumptions are adopted:

- Hydrogen demand is treated as exogenous and follows a deterministic growth projection to provide a baseline for long-term infrastructure planning.
- Technology efficiencies and emission factors are assumed to remain constant across periods.
- Great-circle distances represent transportation distances, and the model does not incorporate a detailed road network structure.
- Unit production costs are treated as deterministic parameters.
- A learning rate of 5% per year is applied to account for cost reductions as technology manufacturers accumulate experience over time.

Table 1. Primary data categories and sources.

Category	Key Parameters	Source
Energy supply	Renewable energy, biofuel, natural gas, and coal potentials	EPDK [43], BEPA [44], TKİ [45]
Transportation Data	Number of heavy-duty vehicles, annual driving distance	TÜİK [46]
Demand Assumptions	Hydrogen Fuel Cell Vehicle (HFCV) penetration rates, vehicle fuel consumption	Almansoori and Shah [22], Almaraz et al. [40], Güler et al. [36]
Techno-Economic Data	Capital and operating cost parameters, and capacity constraints	Almansoori and Shah [22]
Emission Data	Emission factors for production, transportation, and storage	Ochoa Bique et al. [47]

While these assumptions are necessary for a structured long-term analysis, they involve certain limitations. The deterministic nature of demand and static cost parameters may not fully capture the high-frequency fluctuations of the Turkish energy market. To address these limitations, a sensitivity analysis was conducted on unit production costs. This analysis examines the model's response to potential economic volatility. It evaluates how variations in the economic environment influence the optimal configuration and the resulting cost-emission trade-offs of the hydrogen supply chain.

4.3. Carbon Tax Scenarios and Penetration Rates

The carbon tax levels are determined based on the price benchmarks suggested in the International Monetary Fund (IMF) report by Parry et al. [41] to align with Türkiye's 2053 net-zero emissions target. The values are specified for each period in alignment with the model's five-period structure, reflecting a gradual fiscal transition to avoid sudden economic shocks. In Scenario 1, the carbon tax is zero for all periods to serve as a baseline. Scenario 2 introduces a moderate tax structure that increases gradually, reaching the \$75/ton CO_2 threshold by period 4 as a key decarbonization milestone. Scenario 3 follows a more aggressive approach, reaching a higher escalation of \$150/ton CO_2 by the final period to test the network's resilience under stringent regulations. Table 2 presents the period-specific values for each scenario.

Table 2. Carbon tax scenarios by period (\$/ton CO_2).

Scenarios	Periods (Years)				
	t1 (2026–2030)	**t2 (2031–2035)**	**t3 (2036–2040)**	**t4 (2041–2045)**	**t5 (2046–2050)**
S1: No carbon tax	0	0	0	0	0
S2: Moderate carbon tax (gradually increasing)	35	50	65	75	90
S3: Aggressive carbon tax (rapid and high increase)	50	75	100	125	150

Hydrogen-fuel-cell vehicle penetration rates are defined over five periods. They are assumed to be low, that is, 5% between 2026 and 2030, and increase gradually, and to reach 100% by the end of the planning horizon (t5). Explicitly, the rates are 5%, 20%, 50%, 85%, and 100% over periods t1 to t5.

https://doi.org/10.3390/cleantechnol8030085

5. Results and Discussion

In this study, the proposed model was implemented in Python (version 3.11.7) and solved with the Gurobi Optimizer (version 11.0.1) for the case of Türkiye described above. All computational experiments were conducted on a computer equipped with a 13th-generation Intel Core i7 processor and 16 GB of random-access memory (RAM). The proposed MILP model is formulated as a large-scale optimization problem comprising approximately 56,710 total variables (including 16,520 binary variables) and up to 65,250 constraints, depending on the scenario and the AUGMECON2 iteration. The representative Pareto solutions defined in the methodology section, namely the minimum emission solution, the knee point, and the minimum cost solution, are examined in this section in terms of system behavior. First, each solution type is evaluated under the three carbon tax scenarios to analyze infrastructure composition, investment dynamics, technology distribution, spatial concentration, and the cost–emission relationship. Subsequently, the solutions are compared, and the impact of carbon pricing on system outcomes across different infrastructure architectures is discussed.

A total of 20 Pareto-optimal solutions is obtained for each scenario. The complete set of Pareto frontiers for all scenarios is shown in Figure A1 (Appendix A). To facilitate interpretation and comparison, representative solutions corresponding to the extreme points and the knee region of the Pareto curve are selected for detailed analysis. In this context, three reference solutions are as follows:

- The extreme solution representing minimum emissions (A),
- The knee point reflecting a balanced trade-off between cost and emissions (B),
- The extreme solution corresponding to the minimum cost (C).

These representative solutions reflect different transition strategies, depending on their positions within the Pareto solution space and the decision-maker's preferences. Figure 3 conceptually illustrates the approach used to identify these reference solutions from the Pareto-optimal solution set. The objective function values across different scenarios are explained in detail in the following subsections.

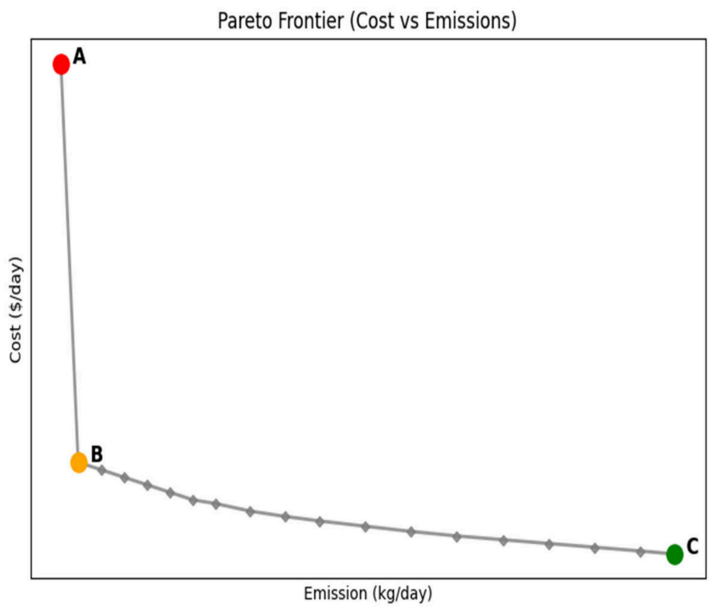

Figure 3. Conceptual illustration of the Pareto-optimal solution space and the selection of representative extreme and knee-point solutions (A–B–C) for further analysis.

5.1. Assessment of Point A (Pareto ID = 0)

Pareto ID = 0 solution demonstrates the supply chain structure with the highest cost and minimum total emissions. The effect of carbon pricing on the Pareto ID = 0 solution manifests primarily as a gradual shift in the system's structural transformation towards hydrogen. In other words, the carbon tax does not serve as a supporting policy for hydrogen production; rather, it increases the total cost of the supply chain. A comparison across scenarios indicates that the LCOH increases as carbon prices rise. The LCOH value, which is 12.36 $/kg H_2 in the no tax scenario (S1), increases to 13.41 $/kg H_2 under the moderate carbon tax (S2) and further to 14.06 $/kg H_2 under the aggressive carbon tax (S3), as shown in Table 3. However, the energy used in the production stage is entirely renewable electricity, and the use of natural gas, coal, and biomass remains zero across all periods. This result indicates that the carbon tax policy does not alter the energy mix but only increases production costs.

Table 3. Key indicators by scenario (Point A, Pareto ID = 0).

Scenario	LCOH ($/kg H_2)	Energy Used in Production
S1	12.36	100% renewable electricity
S2	13.41	100% renewable electricity
S3	14.06	100% renewable electricity

Table 4 presents the total system cost and the corresponding carbon tax payments on a period basis. Given the relatively large scale of total system costs, the tax component appears to be of limited magnitude relative to the overall cost structure. This is because the investment costs for a decentralized supply chain of facilities constitute a large share of total costs, even aggressive carbon taxes (S3 scenario) may not alter this cost breakdown or the technology choice. In addition, in this decentralized supply chain structure, renewable energy usage is already at 100%, and adding higher taxes does not contribute; it only increases the LCOH.

Table 4. Period-wise total system cost and carbon tax rates (ID = 0).

Period	Total Cost ($)	S1	S2	S3
t1	24,147,628,575	0	0.001%	0.002%
t2	69,187,577,665	0	0.003%	0.004%
t3	48,954,927,683	0	0.014%	0.021%
t4	33,584,295,482	0	0.042%	0.070%
t5	13,861,486,258	0	0.155%	0.258%

By evaluating the infrastructure dynamics together, it becomes clear that system growth is driven not by technological change but by the network's physical expansion. The capacity utilization rate of the electrolyzers increases steadily over the periods, rising from around 10% to approximately 44%, as shown in Figure 4. This increase does not indicate a shift to a new production technology. Rather shows that the installed infrastructure is operated more intensively over time.

In the early stages, investments are primarily made for establishing production facilities. In later periods, storage facilities become more dominant (see Figure 4). The simultaneous increase in storage investments and capacity utilization suggests that the system moves from an installation phase to a more mature operational phase.

The spatial distribution of active facilities in the final period indicates that the system does not converge toward a fully homogeneous configuration, as seen in Figure 5. The resulting network structure is neither entirely centralized nor fully decentralized. The dispersion of relatively small-scale facilities across clusters ensures local accessibility, while transportation flows occur along a limited number of corridors. Accordingly, production is organized in a distributed manner, whereas logistics exhibits a partially centralized structure. The transportation structure is single-mode. The total amount of hydrogen transported within the system is 489,081.57 kg, carried entirely by rail, with no road transport. All flows occur exclusively from cluster 5 to cluster 22, and no other transportation corridor becomes active.

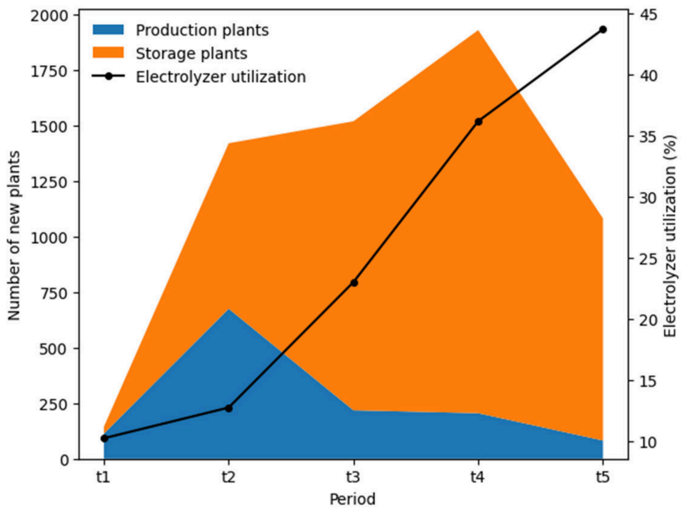

Figure 4. Temporal evolution of production and storage investments together with electrolyzer utilization (Point A, Pareto ID = 0).

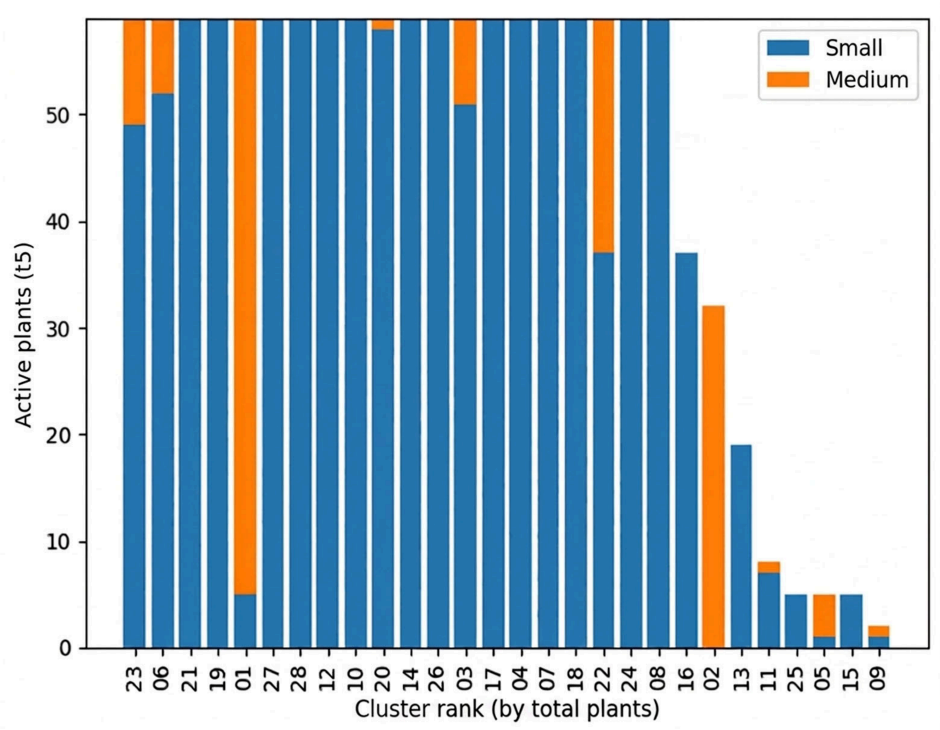

Figure 5. Ranked distribution of active electrolyzer plants by cluster in the final period (t5).

These findings indicate that in the ID = 0 solution, carbon pricing does not change the system structure but only increases the cost level. The energy mix, technology distribution, emission pathway, and infrastructure configuration remain unchanged. In this solution, the carbon price does not alter technology selection; instead, it creates economic pressure that affects the overall cost level and the intensity of system operation.

5.2. Assessment of Point B (Pareto ID = 1)

The Point B (ID = 1) solution represents a significant decrease in total cost compared to that of the Point A, at the expense of a relatively small emission increase, as seen in Figure 3. This solution exhibits a system response that preserves the overall infrastructure structure under carbon pricing, while accommodating limited spatial reallocation of capacity.

A comparison across scenarios shows that total system cost increases from 44.65 million in S1, 53.90 million in S2, to 60.14 million in S3, while the LCOH rises from 6.09 in S1, 7.19 in S2, to 7.88 \$/kg H_2 in S3. In contrast, emission levels remain approximately constant at 120.7 million kg CO_2 across all scenarios. This pattern indicates that the observed cost increase stems from the additional carbon pricing burden, which does not alter the ranking of production technologies. An examination of the period-specific investment profiles reveals that periods t3 and t4 constitute the peak investment phases across all scenarios, as shown in Figure 6. Storage investments remain identical across scenarios, following the sequence 36–36–74–93–71 new storage facilities over five periods. Despite minor differences in production facility investments, the overall expansion pattern remains unchanged.

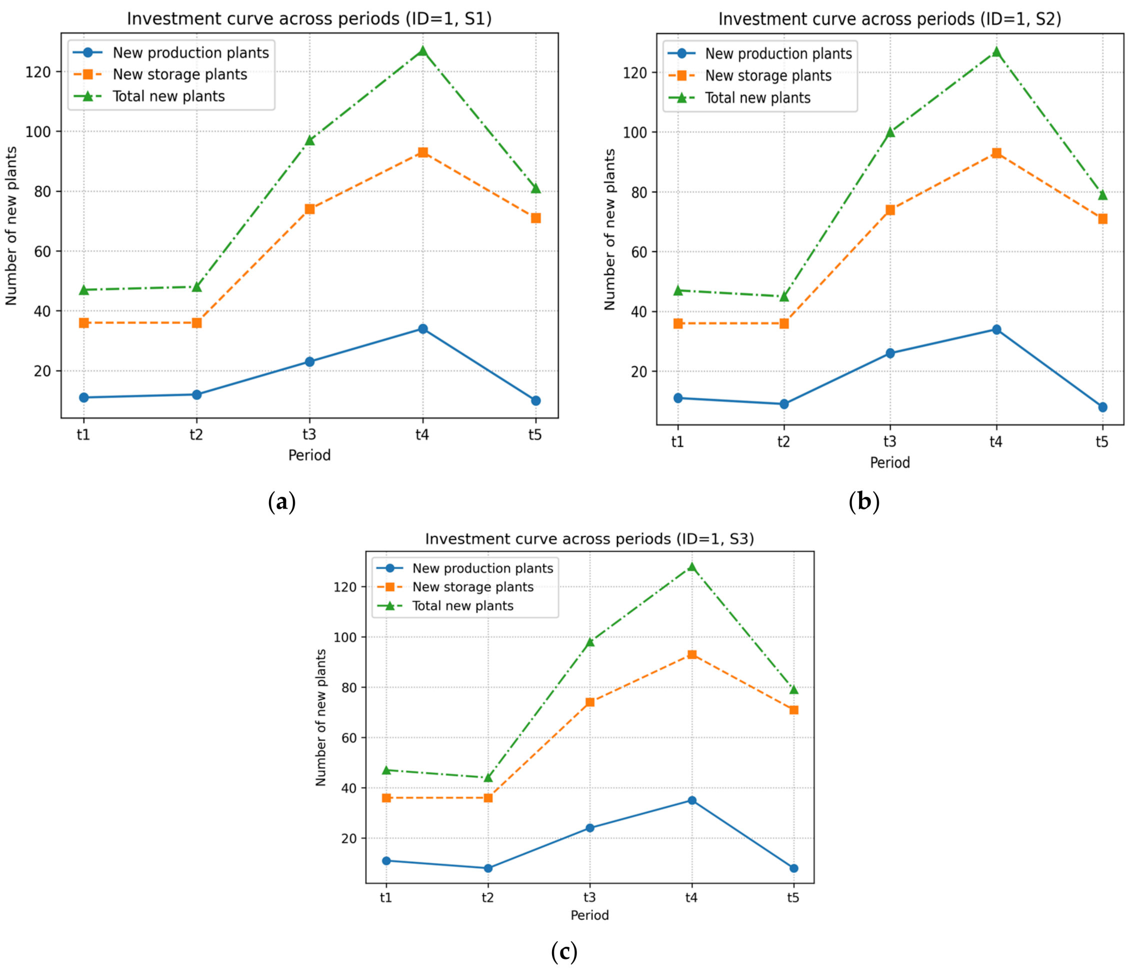

Figure 6. Period-wise number of newly installed production and storage facilities and their total for ID = 1 under S1–S3 scenarios: (**a**) Scenario S1; (**b**) Scenario S2; (**c**) Scenario S3.

The production technology selection indicates that electrolysis is the dominant production component in the hybrid configuration. No new SMR investments occur during periods t2–t4, while SMR facilities are installed only in limited numbers in the initial and final periods. Figure 7 illustrates these results. Despite rising carbon tax levels, the system's backbone technology remains unchanged. Accordingly, the stability of the overall emission level across scenarios is to be expected.

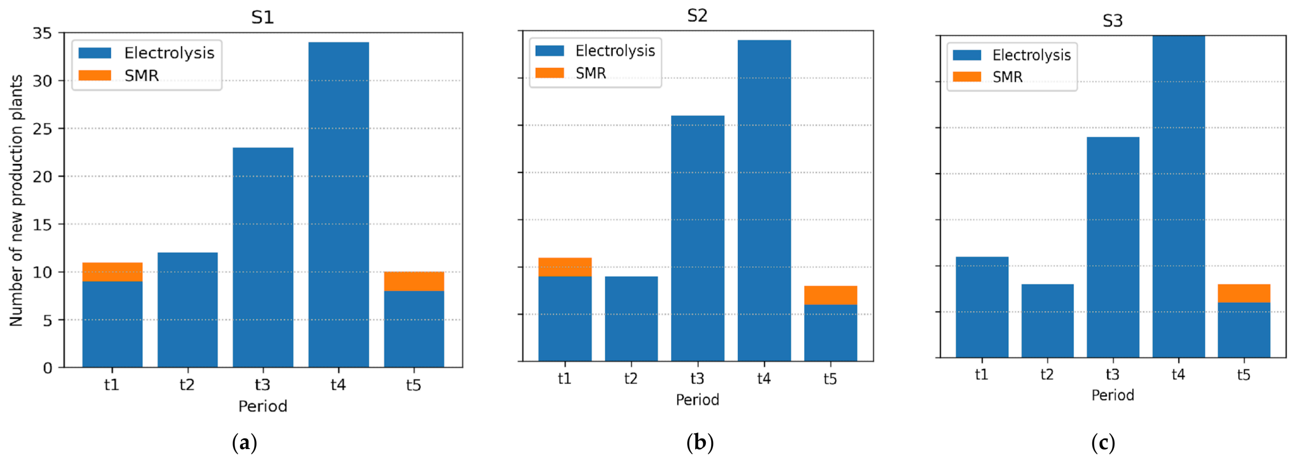

Figure 7. Technology composition of newly installed production facilities for ID = 1 across periods (t1–t5) under S1–S3 scenarios: (**a**) Scenario S1; (**b**) Scenario S2; (**c**) Scenario S3.

When the spatial distribution is examined, within the widespread electrolysis network, certain nodes are preferred. In period t5, medium-scale electrolysis facilities concentrate in specific clusters. However, this concentration is reallocated across scenarios toward nodes that provide relative cost advantages (see Figure 8). Capacity decreases in some nodes while increasing in others, yet the overall distribution pattern is preserved.

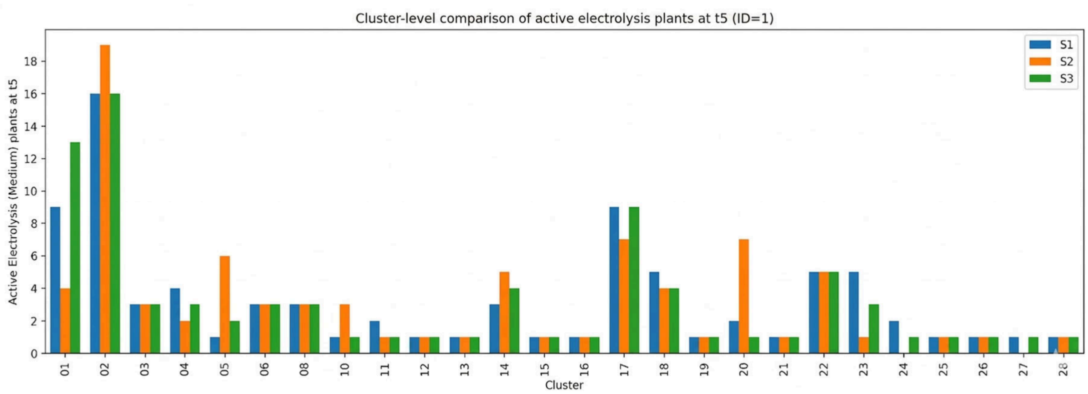

Figure 8. Cluster-level comparison of active medium-scale electrolysis facilities at period t5 for ID = 1 under S1–S3 scenarios.

This pattern becomes more apparent when cluster-level differences are examined. A rebalancing of capacity across specific nodes is observed among the scenarios. Figure 9 shows the change in the number of plants between scenario pairs of S1 and S2, as well as S2 and S3. For instance, compared with S1, Scenario S2 exhibits a reduction in capacity in cluster 1, accompanied by increases in clusters 5 and 20.

Similarly, Scenario S3 yields limited increases at some nodes and decreases at others, compared to S1. These variations indicate that capacity is locally reallocated across clusters, while the overall structural configuration of the system remains largely unchanged. Similarly, SMR facilities exhibit changes in active locations across scenarios only in a limited number of nodes (See Table 5).

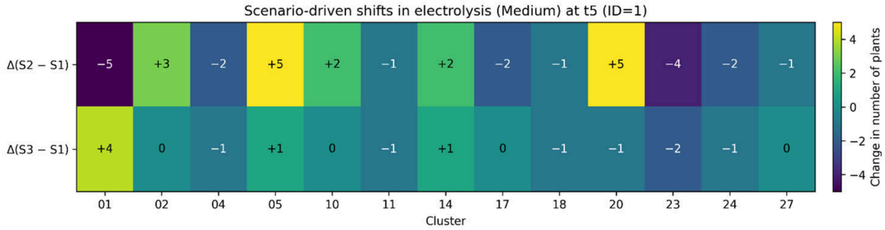

Figure 9. Spatial changes in medium-scale electrolysis installations between scenarios at period t5 for ID = 1.

Table 5. Active SMR plants in period t5 (Point B, Pareto ID = 1).

Scenario	Cluster	Size	Number of Active Plants
S1	01	Large	2
	16	Small	1
	25	Small	1
S2	01	Large	1
	20	Large	1
	16	Small	1
	25	Small	1
S3	01	Large	1
	25	Large	1

By evaluating all findings together, we may conclude that the carbon price in this Pareto solution does not reach a threshold level that would change the ranking of technologies. The system responds to carbon pricing by reallocating capacity spatially rather than through a technological shift. While the emission level remains stable, total cost and LCOH increase, and the infrastructure and production backbone remain unchanged. This is because, in the hybrid supply chain infrastructure, renewable energy is heavily utilized across all scenarios, and a higher carbon tax does not further reduce total emissions. Therefore, this solution shows that under this structure, carbon pricing leads to higher costs rather than emission reduction. The system adapts through spatial marginal-cost optimization rather than technology substitution. This outcome is mainly due to the relatively low-carbon production mix, which prevents the carbon price from altering marginal technology preferences.

A quantitative comparison of the cost-emission trade-offs across scenarios confirms the system's rigidity. In a hybrid configuration that heavily utilizes renewable energy resources, moving from Scenario S1 (No Tax) to S3 (Aggressive Tax) increases the LCOH by 29.06% (from 6.09 to 7.86 \$/kg H_2). Despite this significant economic burden, emissions remain nearly constant at approximately 120.7 million kg of CO_2. This numerical evidence indicates that the system absorbs the carbon tax as a cost penalty rather than responding with a structural technological shift.

5.3. Assessment of Point C (Pareto ID = 19)

The centralized solution (ID = 19) exhibits a hub-and-spoke configuration, with production concentrated in a limited number of nodes and distributed across a broad geographic area. This structure is reflected in the modal distribution of transportation across scenarios: approximately 89–91% of total hydrogen is transported by rail, while only 9–11% is carried by truck, as presented in Table 6. The dominance of rail transport and the distribution of flows from a few central nodes to many destinations indicate that the system does not establish a local production–local consumption match. Instead, it relies on centralized production with large-scale distribution.

Table 6. Transportation mode shares.

Scenario	Truck (%)	Rail (%)
S1	9.44	90.56
S2	10.76	89.24
S3	10.27	89.73

When the spatial, cluster-based distribution of SMR and electrolysis facilities in the final period is evaluated jointly, production capacity is concentrated in a limited number of central nodes. SMR plants are concentrated in only a few clusters, where high-capacity units form the network's main production backbone. Although electrolysis facilities are dispersed across a wider geographic area, they remain relatively few in most clusters. This configuration indicates that, within a structure in which the centralized backbone is preserved, electrolysis primarily serves a complementary role. However, with the introduction of carbon pricing, electrolysis becomes a more visible production component in certain regions. Figure 10 illustrates these results.

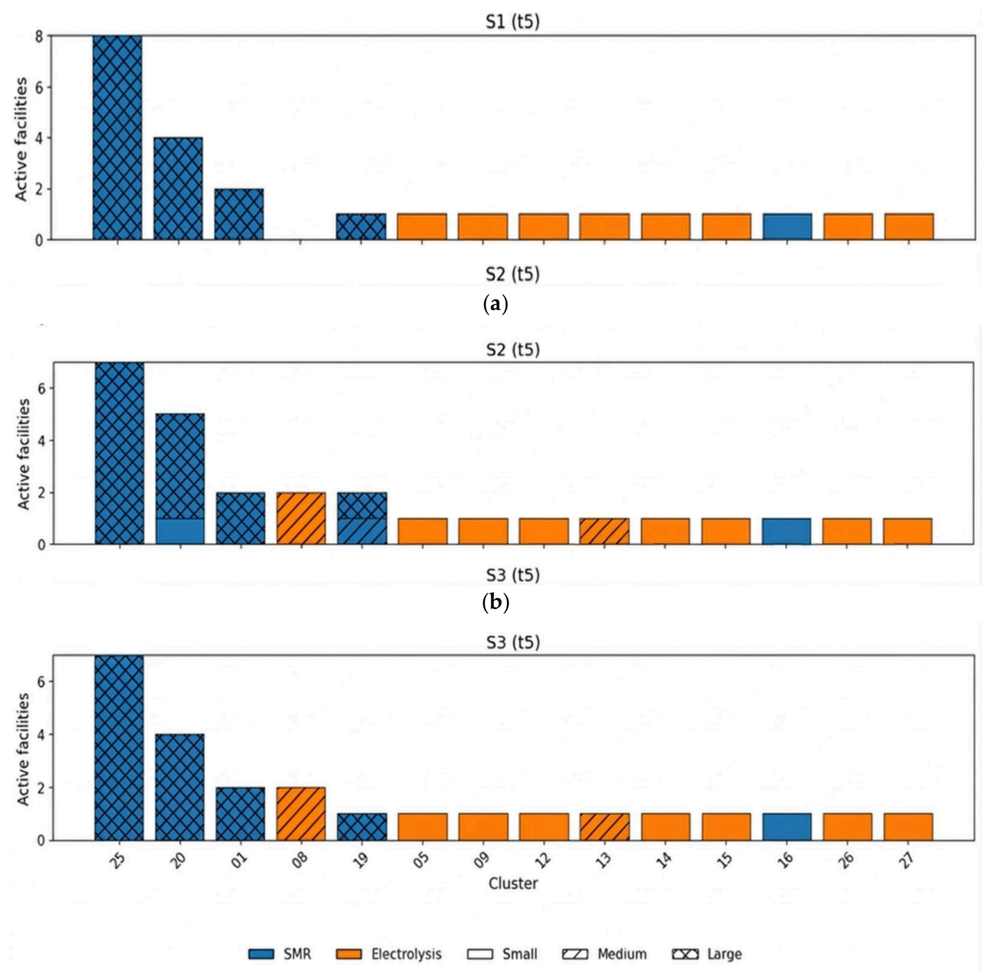

(**a**)

(**b**)

(**c**)

Figure 10. Distribution of active production facilities by cluster, technology, and size in the final period (t5) under S1–S3 scenarios (ID = 19): (**a**) Scenario S1; (**b**) Scenario S2; (**c**) Scenario S3.

The composition of total energy inputs varies significantly across scenarios. In the no-tax case (S1), nearly the entire system's energy demand depends on natural gas (NG), while the share of renewable electricity remains at approximately 2%, as shown in Table 7. Under the carbon pricing scenarios S2 and S3, however, the energy mix undergoes a substantial transformation, with natural gas and renewable electricity converging toward an approximately equal share. Notably, the results for S2 and S3 are very similar. This outcome suggests that once the carbon price exceeds a certain threshold, the major substitution in the energy mix has already occurred, and further increases in the carbon price generate only limited marginal effects on the overall composition.

Table 7. Cumulative energy consumption shares by energy sources across the planning horizon under different carbon tax scenarios.

Scenario	NG (%)	Electricity (%)	Total
S1	97.96	2.04	100
S2	53.03	46.97	100
S3	53.06	46.94	100

Although the distribution of installed capacity remains largely stable across scenarios, the system response emerges primarily at the operational level. SMR facilities continue to operate at high-capacity utilization across all scenarios, whereas the utilization rate of electrolysis facilities increases markedly with the introduction of carbon pricing. This pattern indicates that the system adapts to the carbon constraint not through extensive deployment of new technologies, but rather by adjusting the operational intensity of existing facilities. Figure 11 illustrates these results.

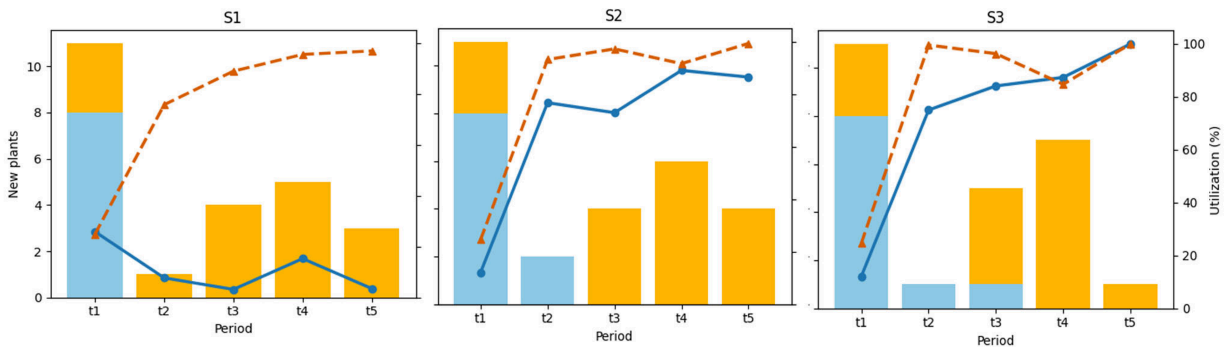

(**a**) (**b**) (**c**)

Figure 11. Newly installed production capacity by technology (stacked bars) and capacity utilization rates (lines) across periods (t1–t5) for the centralized configuration (ID = 19) under S1–S3 scenarios: (**a**) Scenario S1; (**b**) Scenario S2; (**c**) Scenario S3. Blue represents the electrolyzer and orange represents SMR.

Across the scenarios, the LCOH values are realized as 2.06, 4.30, and 5.53 \$/kg H_2, respectively. Although the energy mix remains almost unchanged from S2 to S3, the continued increase in cost indicates that a more aggressive carbon price is directly reflected in operating costs. When the three solution types are evaluated jointly, it becomes evident that the impact of carbon tax scenarios on system behavior varies significantly with the selected infrastructure architecture, as seen in Table 8. Renewable energy shares are the ultimate values at the end of the last period.

Considering all findings together, it becomes clear that carbon pricing does not fully restructure the topology of the centralized network. However, it significantly transforms the system's operating regime. While the core production nodes and the distribution of transport modes remain largely stable, the composition of energy inputs for production and the balance between electrolysis and SMR utilization change meaningfully. In this framework, the system does not build an entirely new infrastructure. Instead, it adjusts the operating levels of existing facilities and makes limited updates in capacity composition in certain nodes to comply with the carbon tax changes. The LCOH value reflects this transformation.

Table 8. Comparative summary of the three solution types across scenarios.

	Scenario	Renewable Energy Share (%)	LCOH ($/kg H_2)	Cost ($)	Emission (kg)
Decentralized configuration (ID = 0)	S1	100.00	12.36	80,383,730	115,152,429
	S2	100.00	13.41	96,608,922	115,152,429
	S3	100.00	14.06	85,429,457	115,152,429
Hybrid configuration (ID = 1)	S1	99.69	6.09	44,647,720	120,712,595
	S2	99.69	7.19	53,904,975	120,714,858
	S3	99.69	7.86	60,135,884	120,715,297
Centralized configuration (ID = 19)	S1	2.05	2.06	14,925,342	226,355,754
	S2	46.98	4.32	33,594,012	220,838,579
	S3	46.96	5.52	44,344,635	220,846,932

5.4. Sensitivity Analysis

In this section, we examine how the proposed hydrogen infrastructure configuration responds to key shifts in the economic, environmental, and policy constraints. Given the long-term planning horizon extending to 2053, certain trends—such as the maturation of electrolyzers and associated energy storage systems—are expected to significantly reduce initial capital expenditures (CAPEX). While these technological learning effects exert a predictable downward pressure on costs, the focus of this analysis is shifted toward more dynamic variables to assess the system's resilience under operational stress.

A ±20% variation was applied specifically to the Unit Production Cost (UPC) of hydrogen from electrolyzer units. Since electricity prices and operational expenses are the primary drivers of green hydrogen, varying the UPC serves as a strategic proxy for assessing the impact of electricity market volatility on the most sensitive part of the supply chain. This analysis, conducted under the aggressive carbon tax scenario (S3), evaluates the resulting trade-offs summarized in Table 9.

Table 9. Sensitivity of system performance and LCOH to electrolyzer unit production cost (UPC) variations.

Scenario	Variable	−20% UPC	Base Case	+20% UPC
ID = 0 (Point A)	System Cost ($)	94,793,804	85,429,457	100,566,797
	Emission (kg CO_2)	115,152,429	115,152,429	115,152,429
	LCOH ($/kg H_2)	13.10	14.06	15.02
	Primary Production Method	Electrolysis	Electrolysis	Electrolysis
ID = 1 (Point B)	System Cost ($)	53,492,228	60,135,884	66,334,118
	Emission (kg CO_2)	120,714,384	120,715,297	120,714,399
	LCOH ($/kg H_2)	7.01	7.86	8.68
	Primary Production Method	Electrolysis and SMR	Electrolysis and SMR	Electrolysis and SMR
ID = 19 (Point C)	System Cost ($)	43,606,201	44,344,635	44,906,829
	Emission (kg CO_2)	226,391,518	220,846,932	220,829,872
	LCOH ($/kg H_2)	5.40	5.52	5.58
	Primary Production Method	Electrolysis and SMR	Electrolysis and SMR	Electrolysis and SMR

The most significant finding of this analysis is the network's structural and environmental invariance. The results demonstrate that fluctuations in UPC of hydrogen from the electrolyzer do not trigger a reconfiguration of the network topology or a shift in the primary technology selection for any of the evaluated Pareto solutions (ID 0, 1, and 19). Furthermore, emission levels remain highly resilient to these cost shifts. This indicates that the network's architecture and environmental performance are governed by stringent emission targets and long-term policy constraints rather than marginal price volatility. In this context, UPC changes are reflected almost exclusively as numerical adjustments in the LCOH rather than as changes in the physical system.

The degree of economic sensitivity, however, depends heavily on the strategic orientation of each Pareto point. The cost-oriented extremity (ID 19) exhibits remarkable economic resilience, with the LCOH rising only marginally from 5.52 \$/kg to 5.58 \$/kg despite a 20% increase in electrolysis costs. This stability is due to hydrogen production in ID 19 already being heavily dominated by SMR-based pathways. Since the model naturally prioritizes the more cost-effective SMR method in this solution, changes to the electrolysis UPC have a negligible impact on the LCOH. Conversely, for the environmentally centric solution (ID 0), where electrolysis is the sole production method, the UPC variation is directly absorbed into the LCOH, thereby shifting it from 13.10 \$/kg to 15.02 \$/kg. Even under significant cost pressure, the system maintains its environmental integrity by accepting a higher unit cost rather than reverting to cheaper, high-emission alternatives. As a result, the analysis demonstrates the structural robustness of the network under the Aggressive carbon tax scenario (S3), where the fundamental infrastructure and environmental targets remain robust despite significant unit production cost changes.

To determine the specific threshold at which the network topology changes, we executed a boundary-condition test. While the spatial layout does not change under standard $\pm 20\%$ cost fluctuations, a 60% reduction in both electrolyzer unit production costs (UPC) and electrolyzer facility capital investment costs (FCC) changes the network configuration. Mathematically, this 60% drop eliminates the cost gap between renewable and fossil fuel options. Because the model naturally seeks to minimize emissions but is constrained by high base-case costs, reducing these costs enables the system to prioritize environmental goals without incurring a major financial penalty. As a result, the low emission targets that previously required high expenditures in the base case (\$85.43 million at Point A) are now achieved at a significantly lower system cost of approximately \$35.01 million across all Pareto points, resulting in significant cost savings compared to the baseline results presented under the S3 scenario in Table 8. The physical network restructures based on these economic alternatives. In the environmentally centric solution (Point A), natural gas consumption drops to zero, and the system selects a layout using Small electrolyzers. In the balanced and cost-oriented steps (Points B and C), the solutions converge. Here, the model shifts toward a configuration with Medium electrolyzers, utilizing the green capacity near its operational limit while restricting SMR to a single marginal unit at Cluster 18. This test proves that a 60% cost reduction is the exact threshold required to align the cost and emission objectives, bringing the overall LCOH boundaries down to \$4.46–7.64/kg H2.

This sensitivity analysis also helps validate the economic necessity of TES integration by quantifying the risks associated with fluctuations in renewable energy output. In this context, the baseline scenario reflects an infrastructure operating without TES support, where fluctuations in renewables cause continuous efficiency losses and intermittent operational penalties, leading to higher LCOH values within each configuration (Table 9). Conversely, the -20% UPC scenario represents a fully integrated TES configuration that mitigates these fluctuations and ensures continuous, high-efficiency operation at the targeted design points. The comparison between these two operational states along the Pareto front demonstrates that TES integration reduces LCOH, thereby empirically justifying its necessity for maintaining grid stability and cost efficiency.

5.5. Discussion

The results indicate that carbon taxation does not produce a consistent linear response in the hydrogen supply chain. The system's response to increased tax levels varies with the initial network structure and production organization, while spatial location decisions are largely unaffected by carbon pricing. Instead, factors like the geographic distribution of resources and existing logistics infrastructure primarily shape production facility locations. Higher carbon taxes do not significantly change this spatial pattern. This observed spatial rigidity indicates that geographic resource availability and logistical proximity act as stronger drivers than fiscal penalties in the Turkish hydrogen context.

To evaluate the external validity of these findings, the structural behavior can be contextualized alongside peer emerging economies such as Mexico and Indonesia, which operate under highly comparable energy infrastructure constraints. Official global energy benchmarks indicate that both nations are actively managing the challenge of increasing renewable energy penetration in their power grids while maintaining a heavy near-term reliance on carbon-intensive fossil fuel baseloads [48,49]. For instance, Türkiye's current grid profile, characterized by a renewable energy penetration rate of approximately 43.4%, positions it dynamically alongside Mexico's natural-gas-dominated infrastructure. Based on 2024 data, fossil fuels account for 76.9% of electricity generation in Mexico, positioning its infrastructure under significant decarbonization pressures [48]. Similarly, this profile shares structural benchmarks with Indonesia's coal-dominated electricity sector, which relied on fossil fuels for 82% of its power while keeping renewable penetration at 18% [49]. Alongside these grid constraints, peer nations share highly similar logistics vulnerabilities in transportation carbon-emission intensity. National decarbonization assessments for Mexico indicate that heavy-duty road transport remains the dominant mode of freight transport, accounting for 70% of all freight ton-kilometers traveled [50]. This heavy reliance makes road transport a disproportionate contributor to national emissions: the transport sector is the country's largest source of greenhouse gases at 23%, with road freight accounting for approximately 40% of total transport CO_2 emissions. Such assessments clearly demonstrate that isolated fiscal penalties, such as removing fossil fuel subsidies, prove insufficient without phased infrastructure integration through the 'Avoid-Shift-Improve' framework, which targets an 86% reduction in sectoral emissions by 2050. These interconnected energy mixes and logistics profiles create identical system-level trade-offs regarding technology selection and capacity expansion when integrating green hydrogen facilities. Thus, the multi-period optimization framework and tiered carbon tax strategies developed in this study provide strategic insights. The infrastructure responses and LCOH sensitivities mapped out under varying economic trajectories can therefore serve as transferable strategic benchmarks for energy and transport planners in developing countries such as Indonesia and Mexico, where balancing clean technology adoption with long-term infrastructure planning is essential.

The impact of a carbon tax is more pronounced in production technology; as taxes rise, some technologies see decreased use, while others are adopted later in the planning horizon, especially in the centralized configurations. This suggests that carbon tax influences production choices rather than acting solely as a prohibitive tool. Solutions initially reliant on fossil fuels show more adjustment in energy mix, while those with a high share of renewables mainly face cost changes rather than structural changes.

The technological rigidity observed in decentralized configurations can be attributed to the dominance of capital expenditures (CAPEX). Since electrolyzers and renewable energy assets require high initial investments, the total system cost is heavily front-loaded. Carbon taxes, acting as operational cost (OPEX) signals, remain insufficient to offset these 'sunk costs' or to justify the decommissioning of existing high-CAPEX infrastructure in favor of alternative technologies. Therefore, the system remains locked into its initial optimal configuration, in which the tax primarily increases the LCOH rather than catalyzing an environmental transition.

Based on these observations, a tiered carbon tax scheme (phased approach) appears more suitable for Türkiye's national industrial conditions than a static radical tax. By implementing a phased approach, Türkiye can avoid the formation of 'green barriers' where high costs hinder the transition before infrastructure reaches maturity. Such a strategy would support SMR with Carbon Capture and Storage (CCS) as a vital bridge technology in the short- to medium-term, protecting industrial competitiveness while the green hydrogen network scales up. Aligning tax escalation with infrastructure readiness, rather than adopting a one-size-fits-all model, can prevent the prohibitive economic shocks observed in early European experiences and ensure a more resilient decarbonization pathway.

Investment timing is also crucial; higher taxes lead to more cautious early reactions and adjustments to align investments with demand growth. Cost and capacity utilization can vary significantly depending on when investments are made, reflecting the hydrogen supply chain's temporal sensitivity to fiscal policy changes.

One of the primary technical hurdles in optimizing these investments, especially within the Turkish power grid, is the inherent volatility of renewable energy. Since the grid still relies heavily on fossil fuels, the fluctuating nature of renewables can compromise electrolyzer efficiency and lead to higher LCOH. To address this, integrating thermal energy storage (TES) emerges as a strategic stability solution. As highlighted by Jia et al. [5], TES can smooth out output fluctuations, thereby enhancing the economics of hydrogen production by ensuring more stable operating conditions for electrolyzers. Additionally, emissions from storage processes remain dominant across scenarios, hindering overall reductions in carbon intensity, even if production emissions decrease. This emphasizes that post-production stages significantly impact both costs and carbon intensity, limiting the effectiveness of carbon taxes on improving environmental performance unless all chain components are addressed.

5.6. Managerial Implications

According to the model results, the following managerial implications are proposed:

- In decentralized configurations characterized by a high share of renewables that minimize emissions, the carbon tax does not alter the technology composition. Still, it increases total costs and LCOH without additional environmental gains. So, under such conditions, aggressive carbon taxes are not suggested. To mitigate these rising costs and improve economic viability, managers and policy-makers should prioritize supporting stability-enhancing technologies such as TES. By smoothing out the inherent volatility of renewable energy, TES allows electrolyzers to operate at higher capacity utilization rates. This stabilization directly reduces LCOH, providing a crucial buffer against the financial pressures of carbon pricing during green hydrogen transitions.
- In hybrid structures, where the cost objective is more prioritized than decentralized structures, the carbon tax does not fundamentally transform the infrastructure, yet it influences the timing of investments. This finding underscores the indirect effects of carbon taxation on investment behavior.
- The centralized architecture, minimizing cost, exhibits comparatively higher policy sensitivity. In scenarios with moderate carbon taxes, significant shifts in energy composition occur, enhancing the system's environmental performance. However, aggressive carbon taxes do not always lead to additional emission reduction. So, properly determining the carbon taxes in cost-oriented centralized architectures is essential for the government.

- Post-production stages can play a decisive role not only in cost but also in carbon intensity. So, in addition to production, the storage and transportation stages must also be decarbonized.
- Especially in developing countries, a gradual and predictable increase in carbon taxation may provide a feasible transition pathway. Sudden, aggressive increases can rapidly raise costs, while structural transformation may not always follow.
- The governmental authorities should design carbon pricing together with infrastructure incentives and investment support mechanisms. A coordinated policy framework between the authorities and private sector actors may enhance the economic sustainability of the hydrogen transition.
- Furthermore, the strategic integration of hydrogen derivatives, such as ammonia, should be considered to enhance the economic resilience of the supply chain. Adopting a 'hydrogen–ammonia synergy' can serve as a vital pathway for Türkiye to reduce high transportation costs and buffer the impacts of carbon taxes. As highlighted by Zhou et al. [39], cross-sectoral coupling paradigms that leverage ammonia as a high-density energy carrier can provide the flexibility needed to mitigate the financial pressures identified in decentralized, renewables-heavy configurations.

6. Conclusions

This study examines how the supply chain infrastructure for hydrogen-fuel-cell vehicles in the heavy-duty transport sector adapts under various carbon tax scenarios within a multi-period, bi-objective optimization framework. The model considers production technology, capacity expansion, storage, and transportation, exploring the trade-offs between cost and emissions through three Pareto-optimal solutions.

The findings reveal that carbon pricing impacts the system differently, depending on the chosen infrastructure design and prioritized objectives. In the distributed, renewables-dominant solution, the carbon tax primarily affects economic outcomes without changing the infrastructure's setup. In the hybrid solution, while the environmental profile remains stable, investment timing is responsive to policy signals. Conversely, in the centralized and cost-sensitive solution, carbon taxation may alter the energy mix, making Pareto-front solutions more sensitive to policy changes. Specifically, the results indicate that LCOH values range from 2.06 to 14.06 \$/kg H_2, with carbon pricing (S3) increasing the LCOH by 29.06% in hybrid designs and raising the renewable share to 46.97% in centralized chains.

These results suggest that the effectiveness of carbon pricing hinges on both the tax level and the initial configuration of the system. Different tax increases can lead to varying responses across infrastructure designs. Sensitivity analysis regarding the network's structural stability demonstrates that a $\pm 20\%$ variation in electrolyzer-based unit production costs does not trigger a network reconfiguration, though it shifts the LCOH values within each respective configuration (Table 9). This structural invariance across the Pareto front is mathematically driven by the weight distribution within the objective function, where multi-period capital expenditures (CAPEX) and fixed network infrastructure costs heavily dominate the total system cost, accounting for over 97.5% of the financial weight across all planning horizons. While operational carbon tax penalties escalate dynamically across the periods due to the increasing carbon tax rates applied to the generated emissions, their relative share remains below 2% of the total cost structure even under the most carbon-intensive configurations. Because the optimization framework evaluates long-term bi-objective trade-offs between cost and emissions under these rising fiscal pressures, the network is established in the earlier planning phases to ensure an economically and operationally viable configuration. Once these capital-intensive spatial allocations are deployed, the marginal impact of carbon pricing within the overall objective

https://doi.org/10.3390/cleantechnol8030085

weight is insufficient to justify a physical reconfiguration of the network layout. Spatial allocation decisions are governed by long-term infrastructure investment dynamics, while subsequent carbon tax increases are absorbed almost exclusively as numerical increments in the LCOH.

In addition, according to the results of the boundary condition test, a minimum 60% reduction in both electrolysis investment costs (CAPEX) and UPC results in a shift in supply chain structure and technology selection, enabling widespread deployment of electrolyzers across all supply chain configurations. This test shows that a 60% cost reduction for electrolyzers is the threshold required to align the cost and emission objectives, bringing the overall LCOH boundaries down to \$4.46–7.64/kg H_2. This finding also implies that advances in electrolysis technologies that reduce investment and operational costs are strongly needed to facilitate the utilization of these clean technologies.

Importantly, significant carbon tax increases do not always lead to greater emissions reductions; they can also result in higher costs and slower investment, indicating that carbon pricing alone may not suffice for transformation. Rather, it should be considered alongside infrastructure design and financing strategies.

Finally, this study concludes that policy recommendations for Türkiye must be tailored to its unique conditions, while the developed multi-period MILP framework serves as a representative and scalable model for other emerging economies, since many developing countries have similar carbon-intensive transportation sectors and increasing renewable energy penetration. By aligning the model with Türkiye's 2030–2053 Hydrogen Strategy milestones (such as the 2 GW and 5 GW electrolyzer targets), this study highlights that a tiered carbon tax policy is essential to avoid economic barriers. A tiered carbon tax policy, starting with lower rates to encourage early-stage SMR-CCS investments and escalating as renewable infrastructure matures, is recommended. This balanced strategy prevents the formation of economic barriers, ensures energy security through transitional fossil-fuel-integrated technologies, and aligns Türkiye's hydrogen strategy with international environmental standards in a sustainable manner. In this context, exploring hydrogen–ammonia synergistic models can further optimize the transition by lowering the cost of long-distance transport and storage, thereby increasing the practical applicability of hydrogen energy in Türkiye's heavy-duty transport sector.

Ultimately, this study highlights that Pareto-optimal solutions represent varied cost-emission trade-offs and policy sensitivities. Future research could enhance this framework by integrating demand uncertainty, incorporating technology cost reductions through learning-by-doing, and evaluating policies within bilevel optimization settings.

Additionally, expanding the model to include multi-objective formulations that account for operational risk minimization or system reliability maximization would provide a more robust basis for strategic planning. Furthermore, exploring the integration of stability-enhancing technologies, such as TES, could provide deeper insights into mitigating renewable energy volatility and further reducing the LCOH in fossil-fuel-dependent grids [5]. In addition to these storage options, incorporating micro-level operational strategies, such as flexible on-grid and off-grid control frameworks, can complement infrastructure configurations and help lower the LCOH. Combining macro-level policy instruments with these micro-level control mechanisms represents a critical future pathway for addressing long-term optimization challenges in developing energy markets.

Author Contributions: Conceptualization, F.E. and Ş.I.S.; methodology, F.E. and Ş.I.S.; software, F.E.; validation, F.E. and Ş.I.S.; formal analysis, F.E. and Ş.I.S.; investigation, F.E. and Ş.I.S.; resources, F.E. and Ş.I.S.; data curation, F.E. and Ş.I.S.; writing—original draft preparation, F.E.; writing—review and editing, F.E. and Ş.I.S.; visualization, F.E.; supervision, Ş.I.S.; project administration, Ş.I.S.; funding acquisition, Ş.I.S. All authors have read and agreed to the published version of the manuscript.

Funding: Istanbul Technical University supported this work with the grant number FHD-2026-48039.

Data Availability Statement: The data of all study is openly available in the file at https://docs.google.com/document/d/1cXzq_A9gMozRfZiw6Gt8R9FaRp8-MA_amr04UCHl4lE/edit?usp=sharing (accessed on 18 May 2026).

Conflicts of Interest: The authors declare no conflicts of interest.

Abbreviations

The following abbreviations are used in this manuscript:

AUGMECON	Augmented ε-Constraint Method
BEPA	Energy Affairs General Directorate
CCS	Carbon Capture and Storage
EPDK	Energy Market Regulation Institution
IEA	International Energy Agency
LCOH	Levelized Cost of Hydrogen
MILP	Mixed Integer Linear Programming
SMR	Steam Methane Reformation
TES	Thermal Energy Storage
TKİ	Turkish Coal Enterprises
TÜİK	Turkish Statistical Institute

Appendix A

Appendix A.1. Model Notation

Table A1. Model indices.

Index	Description
e	Primary energy source
g	Cluster
j	Size of production plants and storage facilities
l	Type of transportation mode
p	Production facility with production technology p
s	Storage facility type with different storage technologies
t	Time period of the planning horizon

Table A2. Model parameters.

Symbol	Description
A^0_{eg}	Initial average availability of primary energy sources e in cluster g (unit/d)
CCF	Capital charge factor—payback period of capital investment (yr)
D^T_{gt}	Total demand in cluster g during time period t (kg/d)
DW_l	Driver wage of transportation mode l ($/hr)
FE^L_l	Fuel economy of transportation mode l within a cluster (km/L)
FE^R_l	Fuel economy of transportation mode l between clusters (km/L)
FP_l	Fuel price of transportation mode l ($/L)
GE_l	General expenses of transportation mode l ($/d)
L^L_g	Local delivery distance within cluster g (km)
$L^R_{gg'}$	Regional delivery distance between clusters g and g' (km)
LR	Learning rate—cost reduction as technology manufacturers accumulate experience (%)
LUT_l	Load/unload time of product for transportation mode l (hr)

Table A2. *Cont.*

Symbol	Description
ME_l	Maintenance expenses of transportation mode l (\$/km)
NP^0_{pjgt}	Initial number of production facilities type p and size j in cluster g
NS^0_{sjgt}	Initial number of storage facilities of type s and size j in cluster g
$PCap^{min}_{pj}$	Minimum production capacity of production facility type p and size j (kg/d)
$PCap^{max}_{pj}$	Maximum production capacity of production facility type p and size j (kg/d)
PCC_{pj}	Capital cost of establishing production facility type p and size j (\$)
PR_t	Penetration factor of hydrogen-fuel-cell vehicles during the time period t (%)
Q^{min}_l	Minimum flow rate of hydrogen by transportation mode l (kg/d)
Q^{max}_l	Maximum flow rate of hydrogen by transportation mode l (kg/d)
$SCap^{min}_{sj}$	Minimum storage capacity of storage facility type s and size j (kg)
$SCap^{max}_{sj}$	Maximum storage capacity of storage facility type s and size j (kg)
SCC_{sj}	Capital cost of establishing storage type s and size j (\$)
SP^L_l	Average speed of transportation mode l within a cluster (km/hr)
SP^R_l	Average speed of transportation mode l between clusters (km/hr)
SSF	Safety stock factor of primary energy sources within a cluster (%)
$TCap_l$	Capacity of transportation mode l (kg/mode)
TMA^L_l	Availability of transportation mode l within a cluster (hr/d)
TMA^R_l	Availability of transportation mode l between clusters (hr/d)
TMC_l	Cost of establishing transportation mode l (\$/mode)
UDC_e	Unit cost of distributing primary energy source e between clusters (\$/unit)
UEC_e	Unit cost of primary energy source e (\$/unit)
UPC_{pj}	Unit production cost for production plant type p and size j (\$/kg)
USC_{sj}	Unit storage cost for storage facility type s and size j (\$/kg/d)
E_p	Emission produced in production facility type p for the production of one kg of hydrogen (kg)
E_s	Emission produced in storage facility type s for the storage of one kg of hydrogen (kg)
E_l	Emission produced by the transportation mode l to transport one kg of hydrogen over a distance of one km (kg)
β	Storage holding period—average number of days' worth of stock (d)
γ_{epj}	Rate of utilization of primary energy source e by plant type p and size j (unit resource/unit product)

Table A3. Model continuous variables.

Symbol	Description
A_{egt}	Average availability of primary energy source e in cluster g during time period t (unit/d)
D^L_{gt}	Demand in cluster g satisfied by local production during time period t (kg/d)
D^I_{gt}	Imported demand to cluster g during time period t (kg/d)
EA_{egt}	Available primary energy source e in cluster g at the beginning of period t
FCC_t	Facility capital cost (\$)
FOC_t	Facility operating cost (\$/d)
L^{avg}_{gt}	Average delivery distance within cluster g during time period t (km)

Table A3. *Cont.*

Symbol	Description
P_{pjgt}	Production rate by plant type p of size j in cluster g during time period t (kg/d)
P^T_{gt}	Total production rate in cluster g during time period t (kg/d)
$Q_{lgg't}$	Flow rate by transportation mode l between clusters g and g' during time period t (kg/d)
S_{sjgt}	Average inventory stored in storage type s and size j in cluster g during time period t (kg)
S^T_{gt}	Total average inventory in cluster g during time period t (kg)
EM_t	Total emissions generated from production activities during period t
ES_t	Total emissions generated from storage operations during period t
ET_t	Total emissions generated from transportation during period t
TCC	Transportation capital cost ($)
TDC	Total daily cost of the network ($/d)
TOC	Transportation operating cost ($/d)

Table A4. Model integer variables.

Symbol	Explanation
IP_{pjgt}	Investment of plants of type p and size j in cluster g during time period t
IS_{sjgt}	Investment of storage facilities of type s and size j in cluster g during time period t
NHP_{pjgt}	Number of plants of type p and size j in cluster g during time period t
NHS_{pjgt}	Number of storage facilities of type s and size j in cluster g during time period t
$NTU_{lgg't}$	Number of transportation units of type l between clusters g and g' in period t

Table A5. Model binary variables.

Symbol	Explanation
$X_{lgg't}$	1 if hydrogen is to be transported from clusters g to g' by transportation mode l during time period t, 0 otherwise
Y_{gt}	1 if hydrogen is to be exported from cluster g during time period t, 0 otherwise
Z_{gt}	1 if hydrogen is to be imported into cluster g during time period t, 0 otherwise

Appendix A.2. Supplemental Technical Data and Cluster Information

Table A6. The 28 clusters defined in Türkiye and the provinces they cover.

Cluster ID	Provinces
C1	İstanbul
C2	Ankara, Kırıkkale
C3	İzmir
C4	Konya, Aksaray, Karaman
C5	Bilecik, Bursa, Yalova

Table A6. *Cont.*

Cluster ID	Provinces
C6	Antalya, Burdur, Isparta
C7	Adıyaman, Gaziantep, Kilis
C8	Adana, Mersin, Osmaniye
C9	Diyarbakır, Şanlıurfa
C10	Kayseri, Kırşehir, Nevşehir, Niğde
C11	Çorum, Giresun, Ordu, Samsun
C12	Gümüşhane, Rize, Trabzon
C13	Artvin, Bayburt, Erzurum, Ardahan, Kars, Erzincan, Iğdır
C14	Elazığ, Malatya, Tunceli, Bingöl
C15	Ağrı, Bitlis, Hakkari, Muş, Van
C16	Batman, Mardin, Siirt, Şırnak
C17	Aydın, Denizli, Manisa, Uşak
C18	Balıkesir, Çanakkale
C19	Bolu, Düzce, Sakarya
C20	Tekirdağ, Kırklareli, Edirne
C21	Kahramanmaraş
C22	Kocaeli
C23	Hatay
C24	Kütahya, Eskişehir, Afyonkarahisar
C25	Karabük, Zonguldak, Bartın
C26	Sivas, Tokat, Yozgat, Amasya
C27	Sinop, Kastamonu, Çankırı
C28	Muğla

Table A7. Distance between clusters.

Cluster ID	1	2	3	4	5	6	7	8	9	10	11	12	13	14	15	16	17	18	19	20	21	22	23	24	25	26	27	28
1	50	378	328	511	85	416	857	715	986	562	666	920	1086	925	1212	1148	312	198	176	165	785	85	822	222	279	607	438	424
2	378	57	548	231	323	355	487	378	609	196	335	580	737	550	842	770	450	516	205	543	415	293	485	251	189	247	182	514
3	328	548	35	541	290	317	931	747	1092	666	882	1128	1282	1068	1366	1270	117	165	422	338	866	355	837	297	551	793	685	172
4	511	231	541	150	432	244	390	213	553	160	468	665	794	548	842	734	425	578	376	665	326	435	314	303	411	355	400	437
5	85	323	290	432	83	332	790	639	926	496	634	888	1050	873	1165	1092	248	201	143	234	718	65	745	137	267	563	416	358
6	416	355	317	244	332	99	628	437	795	394	671	893	1031	791	1086	977	202	399	365	533	567	370	522	206	465	565	534	193
7	857	487	931	390	790	628	155	197	175	296	421	451	511	236	486	356	815	959	691	1021	73	773	168	676	659	354	547	819
8	715	378	747	213	639	437	197	147	371	192	460	581	675	404	678	553	630	791	564	873	152	635	108	514	566	357	498	626
9	986	609	1092	553	926	795	175	371	152	434	440	366	374	135	313	182	976	1106	813	1151	228	901	334	823	759	416	623	988
10	562	196	666	160	496	394	296	192	434	139	315	505	637	403	701	607	553	672	396	726	223	477	295	390	379	202	306	583
11	666	335	882	468	634	671	421	460	440	315	293	255	420	323	568	545	785	834	494	823	373	586	529	585	393	113	232	845
12	920	580	1128	665	888	893	451	581	366	505	255	108	168	234	349	382	1026	1088	749	1076	443	841	608	832	646	336	484	1076
13	1086	737	1282	794	1050	1031	511	675	374	637	420	168	389	276	214	306	1176	1249	912	1243	525	1005	678	987	813	490	651	1219
14	925	550	1068	548	873	791	236	404	135	403	323	234	276	199	298	228	957	1063	749	1089	252	840	403	785	677	326	529	983
15	1212	842	1366	842	1165	1086	486	678	313	701	568	349	214	298	246	154	1254	1357	1036	1375	528	1128	647	1082	953	606	796	1279
16	1148	770	1270	734	1092	977	356	553	182	607	545	382	306	228	154	157	1155	1277	972	1313	410	1062	508	996	905	553	757	1169
17	312	450	117	425	248	202	815	630	976	553	785	1026	1176	957	1254	1155	173	217	356	377	750	310	721	205	482	691	601	113
18	198	516	165	578	201	399	959	791	1106	672	834	1088	1249	1063	1357	1277	217	138	343	173	889	256	891	283	464	760	616	316
19	176	205	422	376	143	365	691	564	813	396	494	749	912	749	1036	972	356	343	103	341	618	93	672	167	129	431	273	453
20	165	543	338	665	234	533	1021	873	1151	726	823	1076	1243	1089	1375	1313	377	173	341	110	949	251	979	365	430	769	592	484
21	785	415	866	326	718	567	73	152	228	223	373	443	525	252	528	410	750	889	618	949	25	701	167	606	588	294	481	760
22	85	293	355	435	65	370	773	635	901	477	586	841	1005	840	1128	1062	310	256	93	251	701	20	742	165	208	523	362	417
23	822	485	837	314	745	522	168	108	334	295	529	608	678	403	647	508	721	891	672	979	167	742	30	617	672	437	595	705
24	222	251	297	303	137	206	676	514	823	390	585	832	987	785	1082	996	205	283	167	365	606	165	617	114	285	497	395	291
25	279	189	551	411	267	465	659	566	759	379	393	646	813	677	953	905	482	464	129	430	588	208	672	285	74	352	162	576
26	607	247	793	355	563	565	354	357	416	202	113	336	490	326	606	553	691	760	431	769	294	523	437	497	352	189	207	743
27	438	182	685	400	416	534	547	498	623	306	232	484	651	529	796	757	601	616	273	592	481	362	595	395	162	207	204	679
28	424	514	172	437	358	193	819	626	988	583	845	1076	1219	983	1279	1169	113	316	453	484	760	417	705	291	576	743	679	30

Table A8. Initial availability of energy sources [38–40].

Cluster ID	Natural Gas (ton/day)	Coal (ton/day)	Biomass (ton/day)	Renewable Electricity (kWh/day)
1	124.16	0	22,911.74	13,623,492.09
2	0	0	32,226.69	3,862,095.89
3	0	0	30,056.11	12,874,514.81
4	0	0	64,380.62	10,861,915.07
5	0	0	16,538.26	11,808,980.82
6	0	0	24,352.50	4,127,976.64
7	1.42	0	18,747.51	1,817,579.45
8	0	0	34,804.30	11,272,877.32
9	0	0	45,436.89	803,845.21
10	0	0	33,920.32	4,933,206.49
11	0	0	30,369.11	7,916,209.72
12	0	0	7350.70	2,725,310.96
13	0	0	50,777.99	9,742,252.73
14	0	0	19,879.42	16,852,127.87
15	0	0	41,731.09	5,670,215.50
16	4.29	0	25,726.52	4,163,246.63
17	0	20,684.93	50,256.14	38,156,016.82
18	1.42	13,452.05	32,287.84	17,701,189.62
19	39.40	0	17,908.05	5,382,724.66
20	759.73	0	28,335.79	12,246,043.84
21	0	0	10,557.35	2,614,383.45
22	0	0	5758.07	949,739.38
23	0.12	0	7928.18	2,676,216.44
24	0	6219.18	35,709.88	5,916,866.14
25	3525.87	0	6131.73	3,510,085.08
26	0	0	38,667.51	5,900,346.83
27	0	0	15,034.07	3,414,202.55
28	0	0	8808.61	2,432,862.47

Table A9. Hydrogen demand of each cluster and time period (t/d).

Cluster ID	t1 (2026–2030)	t2 (2031–2035)	t3 (2036–2040)	t4 (2041–2045)	t5 (2045–2050)
1	111.87	491.25	1339.99	2467.18	3124.99
2	107.60	472.46	1288.75	2372.83	3005.48
3	55.14	242.12	660.45	1216.01	1540.23
4	7.98	35.042	95.59	175.99	222.91
5	3.18	13.98	38.142	70.23	88.95
6	21.75	95.49	260.48	479.59	607.46
7	6.487	28.49	77.70	143.07	181.21
8	19.10	83.87	228.77	421.21	533.51
9	3.87	17.01	46.40	85.43	108.21
10	18.61	81.72	222.90	410.40	519.83
11	5.10	22.380	61.05	112.40	142.37
12	0.85	3.743	10.21	18.80	23.81
13	3.63	15.95	43.51	80.11	101.47
14	1.15	5.047	13.77	25.35	32.10
15	1.56	6.84	18.64	34.33	43.49
16	2.00	8.77	23.91	44.03	55.77
17	7.40	32.50	88.66	163.24	206.76
18	13.71	60.21	164.24	302.39	383.01
19	5.53	24.27	66.19	121.87	154.36
20	3.88	17.06	46.52	85.66	108.49
21	11.42	50.13	136.75	251.78	318.91
22	35.47	155.74	424.82	782.17	990.72
23	26.89	118.09	322.13	593.09	751.23
24	9.32	40.925	111.63	205.54	260.34
25	1.08	4.76	12.99	23.91	30.289
26	3.00	13.19	35.99	66.26	83.92
27	2.39	10.52	28.68	52.81	66.90
28	9.91	43.51	118.69	218.53	276.80

Table A10. Production capacities and costs of hydrogen plants [28,42].

Plant Type, *p*	**SMR**			**CG**		**BG**		**Electrolysis**	
Plant Size, *j*	**S**	**M**	**L**	**M**	**L**	**M**	**L**	**S**	**M**
$PCap_{pj}^{min}$ (t/d)	0.3	10	200	10	200	10	200	0.3	10
$PCap_{pj}^{max}$ (t/d)	9.5	150	960	150	960	150	960	9.5	150
γ_{epj} (unit e/unit i)	4.02	3.34	3.16	5.64	5.33	18.43	11.26	52.49	52.49
PCC_{pj} (\$ × 10^6)	29	224	903	389	1611	575	1836	61	663
UPC_{pj} (\$/kg)	3.36	1.74	1.43	2.03	1.56	3.52	2.15	6.82	5.03

SMR: Steam Methane Reformation, CG: Coal Gasification, BG: Biomass Gasification, S: Small, M: Medium, L: Large.

Table A11. Costs associated with primary energy sources [30].

Primary Energy Source, e	**Natural Gas**	**Coal**	**Biomass**	**Renewable Electricity**
Unit cost of energy source, $\mathrm{UEC_e}$ (\$/unit)	0.12	0.03	0.05	0.05
Unit import cost of energy source, $\mathrm{UIC_e}$ (\$/unit)	0.012	0.003	0.005	0.005
Unit distribution cost of energy source, $\mathrm{UDC_e}$ (\$/unit/km)	1.22×10^{-5}	3.05×10^{-6}	5.09×10^{-6}	5.09×10^{-5}

Table A12. Storage capacities and costs of liquid hydrogen storage facilities [30].

Storage Type, *s*	**Liquid Hydrogen Storage**		
Storage Size, *j*	**Small**	**Medium**	**Large**
Minimum storage capacity, $SCap_{sj}^{min}$ (t)	0.5	10	200
Maximum storage capacity, $PCap_{sj}^{max}$ (t)	9.5	150	540
Storage capital cost, SCC_{sj} (million \$)	5	33	122
Unit storage cost, USC_{sj} (\$/kg/d)	0.032	0.010	0.005

Table A13. CO_2 Emissions per kg of hydrogen produced [47].

Production Technology	**CO_2 Produced kg^{-1} H_2**
Steam Reforming	17.4
Coal Gasification	30.3
Electrolysis	0.9
Biomass Gasification	32.1

Table A14. Costs and characteristics of transportation modes [28,42].

Transportation Mode, *l*	**Tanker Truck**	**Railway Tank Car**
Transport unit capacity, $TCap_l$ (t/mode)	4	9
Fuel economy within cluster, FE_l^L (km/L)	2.30	3.83
Fuel economy between clusters, FE_l^R (km/L)	2.55	4.25
Average speed within cluster, SP_l^L (km/hr)	25	20
Average speed between clusters, SP_l^R (km/hr)	55	45
Mode availability within cluster, TMA_l^L (hr/d)	15	8
Mode availability between clusters, TMA_l^R (hr/d)	18	12
Load/unload time, LUT_l (hr)	2	12
Driver wage, DW_l (\$/hr)	23	23
Fuel price, FP_l (\$/L)	1.16	0.28
Maintenance expenses, ME_l (\$/km)	0.0976	0.0621
General expenses, GE_l (\$/d)	8.22	6.85
Transport mode cost, TMC_l (\$/mode)	500,000	500,000

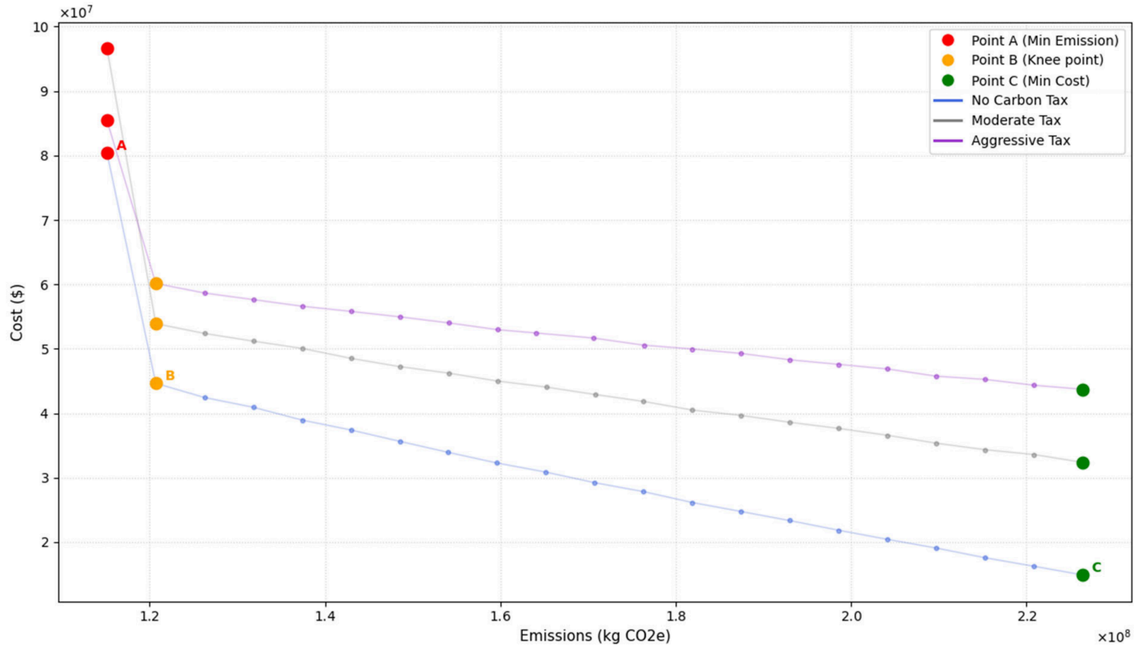

Figure A1. Comparison of Pareto frontiers for total daily system cost and emissions under different carbon tax scenarios. Points A, B, and C represent specific multi-objective optimization solutions illustrating the trade-off between economic and environmental objectives.

References

1. IEA. World Energy Outlook 2022. 2022. Available online: https://www.iea.org/reports/world-energy-outlook-2022 (accessed on 10 February 2026).
2. T.C. Enerji ve Tabii Kaynaklar Bakanlığı. Enerji ve Tabii Kaynaklar Görünümü 2025: Elektrik Piyasası ve Genel Enerji Dengesi İstatistikleri. 2026. Available online: https://enerji.gov.tr/bilgi-merkezi-enerji-elektrik (accessed on 26 April 2026).
3. Li, X.; Ye, T.; Meng, X.; He, D.; Li, L.; Song, K.; Jiang, J.; Sun, C. Advances in the Application of Sulfonated Poly(Ether Ether Ketone) (SPEEK) and Its Organic Composite Membranes for Proton Exchange Membrane Fuel Cells (PEMFCs). *Polymers* **2024**, *16*, 2840. [CrossRef]
4. Wang, Z.; Fan, F.; Zhang, H.; Song, K.; Jiang, J.; Sun, C.; Xue, R.; Zhang, J.; Chen, Z. Flexible On-Grid and Off-Grid Control for Electric-Hydrogen Coupling Microgrids. *Energies* **2025**, *18*, 985. [CrossRef]
5. Jia, T.; Shuai, Y.; Wang, F.; Zhang, H.; Yang, D.; Geng, B.; Li, Q.; Wu, Q.; Xu, Y. Empowering modern power systems with thermal energy storage in China: A comprehensive review. *Renew. Sustain. Energy Rev.* **2026**, *235*, 116937. [CrossRef]
6. Ritchie, H.; Roser, M. Emissions by Sector. Our World in Data 2023. Available online: https://ourworldindata.org/emissions-by-sector (accessed on 30 April 2026).
7. Dündar, A.O.; Kolay, A. Karayolu yük ve yolcu taşımacılığının çevresel sürdürülebilirlik bakımından değerlendirilmesi ve Konya ili sera gazı emisyonunun hesaplanması. *Ömer Halisdemir Üniversitesi İktisadi Ve İdari Bilim. Fakültesi Derg.* **2021**, *14*, 317–334. [CrossRef]
8. European Environment Agency (EEA). Greenhouse Gas Emissions from Transport in Europe. Available online: https://www.eea.europa.eu/en/analysis/indicators/greenhouse-gas-emissions-from-transport (accessed on 30 April 2026).
9. Mckinnon, A. *CO_2 Emissions from Freight Transport: An Analysis of UK Data*; Logistics Research Centre, Heriot-Watt University: Edinburgh, UK, 2010.
10. Meng, X.; Mei, J.; Tang, X.; Jiang, J.; Sun, C.; Song, K. The Degradation Prediction of Proton Exchange Membrane Fuel Cell Performance Based on a Transformer Model. *Energies* **2024**, *17*, 3050. [CrossRef]
11. European Commission. The Draghi Report on EU Competitiveness. 2024. Available online: https://commission.europa.eu/topics/competitiveness/draghi-report_en (accessed on 13 March 2026).
12. Ministry of Energy and Natural Resources (ETKB). Türkiye Hydrogen Technologies Strategy and Roadmap. 2023. Available online: https://enerji.gov.tr/Media/Dizin/SGB/tr/Kurumsal_Politikalar/HSP/ETKB_Hidrojen_Stratejik_Plan2023.pdf (accessed on 3 May 2026).
13. Dursun, E.; Acarkan, B.; Kilic, O. Modeling of hydrogen production with a stand-alone renewable hybrid power system. *Int. J. Hydrogen Energy* **2012**, *37*, 3098–3107. [CrossRef]

14. Genç, M.S.; Çelik, M.; Karasu, I. A review on wind energy and wind-hydrogen production in Turkey: A case study of hydrogen production via electrolysis system supplied by wind energy conversion system in Central Anatolian Turkey. *Renew. Sustain. Energy Rev.* **2012**, *16*, 6446–6460. [CrossRef]
15. Mehmeti, A.; Elezi, E.; Xhebraj, A.; Andoni, M.; Bezo, Y. Is Green Hydrogen a Strategic Opportunity for Albania? A Techno-Economic, Environmental, and SWOT Analysis. *Clean Technol.* **2025**, *7*, 86. [CrossRef]
16. Ozarslan, A. Large-scale hydrogen energy storage in salt caverns. *Int. J. Hydrogen Energy* **2012**, *37*, 14265–14277. [CrossRef]
17. Deveci, M. Site selection for hydrogen underground storage using interval type-2 hesitant fuzzy sets. *Int. J. Hydrogen Energy* **2018**, *43*, 9353–9368. [CrossRef]
18. Gumus, A.T.; Yayla, A.Y.; Çelik, E.; Yildiz, A. A combined fuzzy-AHP and fuzzy-GRA methodology for hydrogen energy storage method selection in Turkey. *Energies* **2013**, *6*, 3017–3032. [CrossRef]
19. Kim, J.; Moon, I. Strategic design of hydrogen infrastructure considering cost and safety using multiobjective optimization. *Int. J. Hydrogen Energy* **2008**, *33*, 5887–5896. [CrossRef]
20. Kim, J.; Lee, Y.; Moon, I. An index-based risk assessment model for hydrogen infrastructure. *Int. J. Hydrogen Energy* **2011**, *36*, 6387–6398. [CrossRef]
21. Almansoori, A.; Shah, N. Design and operation of a future hydrogen supply chain: Snapshot model. *Chem. Eng. Res. Des.* **2006**, *84*, 423–438. [CrossRef]
22. Almansoori, A.; Shah, N. Design and operation of a future hydrogen supply chain: Multi-period model. *Int. J. Hydrogen Energy* **2009**, *34*, 7883–7897. [CrossRef]
23. Agnolucci, P.; Akgul, O.; McDowall, W.; Papageorgiou, L.G. The importance of economies of scale, transport costs and demand patterns in optimising hydrogen fuelling infrastructure: An exploration with SHIPMod (Spatial hydrogen infrastructure planning model). *Int. J. Hydrogen Energy* **2013**, *38*, 11189–11201. [CrossRef]
24. Moreno-Benito, M.; Agnolucci, P.; Papageorgiou, L.G. Towards a sustainable hydrogen economy: Optimisation-based framework for hydrogen infrastructure development. *Comput. Chem. Eng.* **2017**, *102*, 110–127. [CrossRef]
25. Kim, M.; Kim, J. Optimization model for the design and analysis of an integrated renewable hydrogen supply (IRHS) system: Application to Korea's hydrogen economy. *Int. J. Hydrogen Energy* **2016**, *41*, 16613–16626. [CrossRef]
26. Ochoa Bique, A.; Zondervan, E. An outlook towards hydrogen supply chain networks in 2050—Design of novel fuel infrastructures in Germany. *Chem. Eng. Res. Des.* **2018**, *134*, 90–103. [CrossRef]
27. Kaiser, R.; Chowdhury, A.M. Hydrogen-Powered Marine Vessels: A Rewarding yet Challenging Route to Decarbonization. *Clean Technol.* **2025**, *7*, 68. [CrossRef]
28. Ogumerem, G.S.; Kim, C.; Kesisoglou, I.; Diangelakis, N.A.; Pistikopoulos, E.N. A multi-objective optimization for the design and operation of a hydrogen network for transportation fuel. *Chem. Eng. Res. Des.* **2018**, *131*, 279–292. [CrossRef]
29. De-León Almaraz, S.; Azzaro-Pantel, C.; Montastruc, L.; Domenech, S. Hydrogen supply chain optimization for deployment scenarios in the Midi-Pyrénées region, France. *Int. J. Hydrogen Energy* **2014**, *39*, 11831–11845. [CrossRef]
30. Almansoori, A.; Shah, N. Design and operation of a stochastic hydrogen supply chain network under demand uncertainty. *Int. J. Hydrogen Energy* **2012**, *37*, 3965–3977. [CrossRef]
31. Nunes, P.; Oliveira, F.; Hamacher, S.; Almansoori, A. Design of a hydrogen supply chain with uncertainty. *Int. J. Hydrogen Energy* **2015**, *40*, 16408–16418. [CrossRef]
32. Dayhim, M.; Jafari, M.A.; Mazurek, M. Planning sustainable hydrogen supply chain infrastructure with uncertain demand. *Int. J. Hydrogen Energy* **2014**, *39*, 6789–6801. [CrossRef]
33. Almansoori, A.; Betancourt-Torcat, A. Design of optimization model for a hydrogen supply chain under emission constraints—A case study of Germany. *Energy* **2016**, *111*, 414–429. [CrossRef]
34. Talebian, H.; Herrera, O.E.; Mérida, W. Policy effectiveness on emissions and cost reduction for hydrogen supply chains: The case for British Columbia. *Int. J. Hydrogen Energy* **2021**, *46*, 998–1011. [CrossRef]
35. Sagastume Gutiérrez, A.; Cabello Eras, J.J.; Otero Meza, D.D. The Energy Transition in Colombia: Government Projections and Realistic Scenarios. *Clean Technol.* **2025**, *7*, 96. [CrossRef]
36. Güler, M.G.; Geçici, E.; Erdoğan, A. Design of a future hydrogen supply chain: A multi period model for Turkey. *Int. J. Hydrogen Energy* **2021**, *46*, 16279–16298. [CrossRef]
37. Erdoğan, A.; Geçici, E.; Güler, M.G. Design of a future hydrogen supply chain: A multi-objective model for Turkey. *Int. J. Hydrogen Energy* **2023**, *48*, 11775–11789. [CrossRef]
38. Tian, M.H.; Hu, Y.J.; Li, C.; Tao, Y.; Wang, H. The development pathway for hydrogen fuel cell heavy-duty trucks in China: An energy-environment-economy life cycle assessment approach. *Energy* **2025**, *322*, 135797. [CrossRef]
39. Zhou, J.; Fan, F.; Ye, X.; Wang, Z.; Xu, J.; Zhang, H.; Jiang, J.; Xue, R.; Sun, C.; Song, K.; et al. Power-to-hydrogen-ammonia coordination and planning for integrated energy systems with ammonia co-firing and waste heat recovery. *Appl. Energy* **2026**, *406*, 127258. [CrossRef]

40. De-León Almaraz, S.; Azzaro-Pantel, C.; Montastruc, L.; Boix, M. Deployment of a hydrogen supply chain by multi-objective/multi-period optimisation at regional and national scales. *Chem. Eng. Res. Des.* **2015**, *104*, 11–31. [CrossRef]
41. Parry, I.; Minnett, D.; Zhunussova, K. *Climate Mitigation Policy in Türkiye*; IMF Working Papers: Washington, DC, USA, 2023; Volume 2023.
42. Mavrotas, G.; Florios, K. An improved version of the augmented ε-constraint method (AUGMECON2) for finding the exact Pareto set in multi-objective integer programming problems. *Appl. Math. Comput.* **2013**, *219*, 9652–9669. [CrossRef]
43. Enerji Piyasası Düzenleme Kurumu (EPDK). Doğal Gaz Yıllık Sektör Raporu. 2026. Available online: https://www.epdk.gov.tr/Detay/Icerik/3-0-94-1007/dogal-gazyillik-sektor-raporu (accessed on 10 February 2026).
44. Enerji İşleri Genel Müdürlüğü. BEPA—Biyokütle Enerji Potansiyel Atlası. 2026. Available online: https://bepa.enerji.gov.tr/ (accessed on 10 February 2026).
45. Türkiye Kömür İşletmeleri (TKİ). Ana Sayfa. 2026. Available online: https://www.tki.gov.tr/ (accessed on 10 February 2026).
46. Türkiye İstatistik Kurumu (TÜİK). Ana Sayfa. 2026. Available online: https://www.tuik.gov.tr/ (accessed on 10 February 2026).
47. Ochoa Bique, A.; Maia, L.K.K.; La Mantia, F.; Manca, D.; Zondervan, E. Balancing costs, safety and CO2 emissions in the design of hydrogen supply chains. *Comput. Chem. Eng.* **2019**, *129*, 106523. [CrossRef]
48. International Energy Agency (IEA). *Mexico Electricity Profile: Generation Mix and Sector Analysis*; IEA: Paris, France, 2024. Available online: https://www.iea.org/countries/mexico/electricity (accessed on 16 May 2026).
49. Ember. *Indonesia Electricity Transition Insights*; Ember: London, UK, 2026; Available online: https://ember-energy.org/countries-and-regions/indonesia/ (accessed on 16 May 2026).
50. Ruiz, A.; Olea, F.; Montalvo, A.F.; García, E. *A Pathway for a Green Transition of the Transport Sector in Mexico: Feasible Interventions That Are Environmentally, Economically, and Socially Beneficial*; World Resources Institute (WRI) México: Mexico City, Mexico, 2023; Available online: https://es.wri.org/sites/default/files/Issue%20Brief-%20Descarbonización-250923_0.pdf (accessed on 16 May 2026).

https://doi.org/10.3390/cleantechnol8030085